Non-metal Alkylsilyl Compounds as Precursors in Atomic Layer Deposition of Chalcogenides and Pnictides

Tiina Sarnet

Laboratory of Inorganic Chemistry
Department of Chemistry
Faculty of Science
University of Helsinki
Helsinki, Finland

Academic Dissertation

To be presented, with the permission of the Faculty of Science of the University of Helsinki, for public criticism in Auditorium A110 of the Department of Chemistry (Chemicum) on December 21st 2015 at 12 o'clock noon.

Helsinki 2015

Supervisors

Professor Mikko Ritala

and

Professor Markku Leskelä

Laboratory of Inorganic Chemistry

Department of Chemistry

University of Helsinki

Helsinki, Finland

Reviewers

Professor Harri Lipsanen

Department of Micro- and Nanosciences

School of Electrical Engineering

Aalto University

Espoo, Finland

Doctor Claudia Wiemer

Laboratorio MDM

Institute for Microelectronics and Microsystems

National Research Council (CNR)

Agrate Brianza, Italy

Opponent

Professor Kornelius Nielsch

Institute for Metallic Materials

Leibniz Institute of Solid State and Materials Research Dresden

Dresden, Germany

ISBN 978-951-51-1821-9 (paperback)

ISBN 978-951-51-1822-6 (PDF version)

http://ethesis.helsinki.fi/

Unigrafia

Helsinki 2015

"Inspiration is the momentary cessation of stupidity."

Abstract

Materials are crucial to the technological advances of society. The never ending need for data storage and new energy sources pushes research towards clear goals. Perhaps some of today's solutions can in the future be replaced or augmented with phase change memories and thermoelectric materials. Phase change materials store data in their amorphous and crystalline phases that have great differences in their electrical and optical properties. Thermoelectric materials can utilize waste heat and produce electricity from temperature differences. They can also be utilized in temperature control as they can be used to create a temperature difference by using electricity.

Shrinking device sizes and increasing device complexity require that deposition methods such as atomic layer deposition (ALD) are used. ALD is based on sequential, saturative surface reactions. Precursors are brought to the surface one at a time, separated by purges. Because of the saturative reactions, each ALD cycle deposits a constant amount of material up to a monolayer, making film thickness control very simple.

ALD of chalcogenides has focused mainly on sulfides, and the chemistries for selenide and telluride depositions have been limited. Pnictides have a similar situation. The ALD chemistries for arsenides include only a few combinations of precursors, and antimonides are barely demonstrated. This is why a new group of precursors was needed. The alkylsilyl non-metal precursors react very efficiently with metal halides in a dehalosilylation reaction. These types of reactions have now been utilized in both chalcogenide and pnictide thin film growth.

In this thesis, several chalcogenide and pnictide ALD processes were studied in detail by utilizing the appropriate alkylsilyl non-metal precursors. In general, typical ALD characteristics were found. Growth rates saturated with respect to precursor pulse lengths; film thicknesses increased linearly with the number of deposition cycles; and the films were stoichiometric with low impurity contents. Application wise, the ALD chalcogenide and pnictide films had the required properties. The phase of the phase change materials could be repeatably and quickly changed, and the thermoelectric films showed a proper response to a temperature gradient.

Preface

The natural sciences, and especially chemistry, have always been my favorite subjects at school. I must thank my teachers Mrs. Anja Peitola for bringing out the joy of chemistry and teaching the basic skills needed later on, and Dr. Elina Näsäkkälä for for letting us roam free in the lab.

During my studies at the university, it became abundantly clear that inorganic chemistry was the only way to go. This feeling became stronger after a couple of summer jobs at the laboratory. In the end, I never left.

My supervisors Prof. Mikko Ritala and Prof. Markku Leskelä are thanked for sharing their seemingly endless knowledge about the elements, and ALD in particular. It has been a privilege to learn from you during these years.

I am deeply grateful for the insightful and constructive comments of the official reviewers of this thesis, Prof. Harri Lipsanen and Dr. Claudia Wiemer. My work was greatly improved due to your suggestions.

In research, no one is an island. There have been so many people who had a large part in this work. The following co-authors and collaborators are thanked for their involvement in this work. I would like to thank Dr. Viljami Pore for initially introducing me to the world of ALD, Mr Timo Hatanpää for his synthetic genius and preparing all the alkylsilyl precursors used during this research, and Dr. Marianna Kemell for her vast knowledge relating to the SEM and EDX. In addition, I am grateful to Dr. Marko Vehkamäki for his expertise with the TEM and electrical characterizations; Dr. Esa Puukilainen and Mr. Miika Mattinen for atomic force microscopy; Dr. Jani Hämäläinen for sharing his knowledge of the inner workings of our reactors; Dr. Kjell Knapas for knowledge on all things chemistry; and Mr. Robert Huggare for breathing life into my ailing reactor. Special thanks go to Mr. Mikko J. Heikkilä, for his tireless help with everything relating to x-rays.

Many people outside our laboratory have greatly contributed to this work. Prof. Timo Sajavaara and Dr. Mikko Laitinen from the University of Jyväskylä as well as Dr. Kenichiro Mizohata from the Material Physics Division are thanked for film composition analysis. I would like to thank Prof. Jouni Ahopelto and Mr. Timo Flyktman from VTT for thermoelectic characterizations. The help with LEIS and its intricacies from Mr. Rik ter Veen of Tascon is greatly appreciated. Dr. Alejandro Schrott, Dr. Yu Zhu and Dr. Huai-Yu Cheng from IBM and Macronix are thanked for their assistance with phase change related measurements. My heartfelt thanks go also to Dr. Simone Raoux from the Helmholtz-Zentrum Berlin for not only the research collaboration,

but especially for the knowledge shared and all the fruitful conversations along the years. Mr. Howard McKee is thanked for his expertise in the English language, for proofreading this thesis and some of the articles it consists of.

The long-term financial support from ASM Microchemistry, and the support from the Finnish Centre of Excellence in Atomic Layer Deposition is gratefully acknowledged. Furthermore, I am most thankful of the Kemian Päivien Säätiö for awarding me a personal grant for my studies.

Of course I would like to thank all present and former colleagues at the Laboratory of Inorganic Chemistry for fruitful work-related conversations, for the completely absurd discussions and especially for the silly jokes. In addition, thanks are due to everyone playing floorball on Fridays. What better way to end a stressful week at work than to tackle a co-worker or a supervisor during a game.

The effect of peer support can never be underestimated. I have met some very special people along the years. Timo, you have been there for literally most of my life, and I hope we will have even more to reminisce about in the coming years. Thanks to Tatu, Reeta, Sonja and all the others involved with Esitisle and HYK. It was a welcome distraction from all the studying. Special thanks go to my partner in crime, Miia. We have been together since we were still young and innocent first year chemistry students, and still share an office. We have vented frustration, laughed at various shenanigans, and eaten enough chocolate throughout the years.

I owe my deepest gratitude to my parents, who have encouraged me in everything I do. I can only say I have tried to make the best of the chances I have gotten. The bragging rights are truly yours.

In the end, I would like to express my most sincere appreciation and love to my fiancé Jason. You kept me remotely sane and functional in the darkest depths of thesis desperation, made me laugh every day, and took me out of the house when I was going stir crazy. It is time to get a life now.

Helsinki, November 2015

Tiina Sarnet

List of original publications

This doctoral dissertation consists of a summary and of the following publications, which are referred to in the text by their Roman numerals. The author's contribution to the publications is described in the indentations.

I **Atomic Layer Deposition of Antimony and its Compounds Using Dechlorosilylation Reactions of Tris(triethylsilyl)antimony**
Viljami Pore, Kjell Knapas, Timo Hatanpää, Tiina Sarnet, Marianna Kemell, Mikko Ritala, Markku Leskelä and Kenichiro Mizohata *Chem. Mater.* **23**, 247 (2011)

The author planned and conducted the deposition experiments with V.P., and analyzed most of the thin films with M.K.. T.H. synthesized the alkylsilyl precursor. K.K. perfomed the *in-situ* reaction mechanism studies. V.P. and K.K wrote the paper, with other authors contributing.

II **Atomic Layer Deposition and Characterization of GeTe Thin Films**
Tiina Sarnet, Viljami Pore, Timo Hatanpää, Mikko Ritala, Markku Leskelä, Alejandro Schrott, Yu Zhu, Simone Raoux and Huai-Yu Cheng *J. Electrochem. Soc.* **152**, D694 (2011)

The author planned and conducted the deposition experiments and performed most of the analysis on the films. T.H. synthesized the alkylsilyl precursor. Laser testing and resistivity experiments were performed by A.S., Y.Z., S.R. and H-Y.C. The author wrote the first draft, and finalized the paper together with other co-authors.

III **Atomic Layer Deposition and Characterization of Bi_2Te_3 Thin Films**
Tiina Sarnet, Timo Hatanpää, Esa Puukilainen, Miika Mattinen, Marko Vehkamäki, Kenichiro Mizohata, Mikko Ritala and Markku Leskelä *J. Phys. Chem. A* **119**, 2298 (2015)

The author planned and conducted the deposition experiments and performed most of the analysis on the films. T.H. synthesized the alkylsilyl precursor. AFM analysis was performed by E.P. and M.M., TEM analysis by M.V. and TOF-ERDA by K.M.. The author wrote the first draft, and finalized the paper together with M.R.

IV **$(Et_3Si)_2Se$ as a Precursor for Atomic Layer Deposition: Growth Analysis of Thermoelectric Bi_2Se_3**
Tiina Sarnet, Timo Hatanpää, Marko Vehkamäki, Timo Flyktman, Jouni Ahopelto, Kenichiro Mizohata, Mikko Ritala and Markku Leskelä *J. Mater. Chem. C*, **3**, 4820 (2015)

The author planned conducted the deposition experiments and performed most of the analysis on the films. T.H. synthesized the alkylsilyl precursor. TEM analysis was performed by M.V., TOF-ERDA by K.M., and electrical characterization by T.F. and J.A.. The author wrote the first draft, and finalized the paper together with M.R.

V **Alkylsilyl Compounds as Enablers of Atomic Layer Deposition: Analysis of $(Et_3Si)_3As$ Through the GaAs Process**
Tiina Sarnet, Timo Hatanpää, Mikko Laitinen, Timo Sajavaara, Kenichiro Mizohata, Mikko Ritala and Markku Leskelä **Submitted**, (2015)

The author planned and conducted the deposition experiments and performed most of the analysis on the films. T.H. synthesized the alkylsilyl precursor. TOF-ERDA and RBS analysis was performed by M.L., T.S. and K.M.. The author wrote the first draft, and finalized the paper together with M.R. and M.L..

List of abbreviations

AFM	atomic force microscopy
AIST	Ag−In−Sb−Te alloys
ALD	atomic layer deposition
ALE	atomic layer epitaxy
CD	compact disc
CVD	chemical vapor deposition
DRAM	dynamic random access memory
DVD	digital versatile disk
EDX	energy dispersive x-ray analysis
FESEM	field-emission scanning electron microscopy
FIB/SEM	focused ion beam/scanning electron microscope
GIXRD	grazing-incidence x-ray diffraction
GST	Ge−Sb−Te alloys
HTXRD	high-temperature x-ray diffraction
LED	light-emitting diode
LEIS	low-energy ion-scattering
MBE	molecular beam epitaxy
ML	monolayer
MOCVD	metal-organic chemical vapor deposition
MOSFET	metal-oxide-semiconductor field-effect transistor
MOVPE	metal-organic vapor phase epitaxy
P	power
PEALD	plasma-enhanced atomic layer deposition
PGEC	phonon glass, electron crystal
PLA	pulsed laser ablation
R	reflectivity
S	Seebeck coefficient
T	temperature
TEM	transmission electron microscopy
TFEL	thin film electroluminescent display
thd	2,2,6,6-tetramethyl-3,5-heptanedione
TMDC	transition metal dichalcogenide
TOF-ERDA	time-of-flight elastic recoil detection analysis
UHV	ultra high vacuum
VLS	vapor-liquid-solid
XRD	x-ray diffraction
XRR	x-ray reflection
ZT	thermoelectric figure of merit
κ	thermal conductivity
κ_e	electronic component of thermal conductivity
κ_p	phononic component of thermal conductivity
ρ	electrical resistivity
σ	electrical conductivity

Contents

Chapter 1

Introduction

Materials engineering or materials development has been an integral part in pushing mankind forward. Learning how to make bronze and iron has furthered the human race by giant leaps. In the modern era, many of the great technological improvements of the 20th century have centered around silicon-based electronics. Our lives have been greatly transformed in just a few decades. As Moore's law is still valid to describe the development in the electronics industry, and green thinking permeates all aspects of life, new and innovative solutions and materials are needed to fulfill increasingly difficult demands.

As society becomes progressively digitalized, more and more storage capacity is needed to store the great variety of data that are constantly produced. Memory these days needs to be fast, non-volatile, durable, rewritable and cheap. One candidate for a new memory concept is phase change memory. Phase change materials were discovered in the 1960s and entered the consumer market in CDs and DVDs a few decades later. A more recent application is the phase change random access memory. The data are stored as zeros and ones by the crystalline and amorphous phase of the material. Phase change materials have a large contrast in electrical and optical properties between the phases, making readout very simple. Rewriting is also easy by changing the phase. Phase change materials are mostly chalcogenide and pnictide materials.

Energy is an important supporter of our way of life. Our society does not function without electricity, and neither do smartphones and air-conditioners. Energy needs to be supplied to the most remote corners of the Earth, and at the same time, excess heat is released from factories and electronic devices without further utilization. Thermoelectric materials create electricity from a temperature difference and can also use electricity to create a temperature difference. Due to simple and robust device structures, thermoelectrics are used in various applications

from Voyager space probes to car-seat coolers. Many of the most used thermoelectric materials belong to the class of chalcogenide and pnictide materials.

Although the material properties utilized in the aforementioned applications are different, the compositions are not. Phase change materials and thermoelectrics are mainly chalcogenides and pnictides, compounds formed by the elements of groups 15 and 16 such as selenides, tellurides, antimonides and arsenides.

The motivation for scientific research can come from various sources; the researcher can, for example focus on interesting scientific questions using curiosity as the main driver. Motivation can also come from striving towards a desired end result. ALD research fits well into the middle of these two extremes. Thin film research stems from fundamental chemical research in finding new chemistries to deposit materials. In addition, clear goals and specifications can be inferred from the applications.

Thin film research has become increasingly important for the microelectronics industry due to the decrease in feature sizes and transformations towards three dimensional substrates. If the developmental pace of the industry continues, new technologies, such as ALD, are needed to face the challenges as much as new materials are required for the changing environment.

This thesis describes a process that started from a clear application, phase change memories, and progressed to basic research in trying to determine the correct chemistry to fulfill the expectations. Phase change materials, such as $Ge_2Sb_2Te_5$, contain elements that were not common in ALD, especially germanium and antimony. Additionally, telluride chemistries, and those of chalcogenides in general, were quite simple and rare.

From this background, the alkylsilyl compounds were found, along with their efficient dehalosilylation reactions [1]. This approach was extended to many non-metals, mainly the chalcogens and pnictogens. Further research could then be extended to other industrially relevant materials, such as thermoelectrics and III-Vs, with the same chemistry.

The structure of this thesis follows the progress of the research from the desired end results to the chemistry that was needed to achieve them and to the results that followed. Chapter 2 describes in detail the materials classes that were the desired outcome, starting with phase change materials that started this whole avenue of research. Chapter 3 describes the main scientific method for this thesis, ALD, and the chemistry behind it. A brief summary of the experimental procedures for depositing and analyzing thin films is given in Chapter 4. Selected results of the alkylsilyl-enabled ALD processes are presented in Chapter 5. Conclusions from the research and some further outlooks are discussed in Chapter 6.

Chapter 2

Introduction to chalcogenide and pnictide materials

Chalcogens are elements from group 16 (6A), comprising sulfur, selenium and tellurium. When discussing chalcogens, oxygen and polonium are usually disregarded. Pnictogens are elements from group 15 (5A), and include nitrogen, phosphorus, arsenic and antimony. Chalcogenides and pnictides are thus compounds formed by these elements.

Chalcogenide and pnictide compounds form an interesting whole, consisting of several industrially relevant material categories. These include phase change materials, thermoelectric materials, topological insulators, along with II-VI and III-V semiconductors. What makes them intriguing is the fact that the same compound can have properties from more than one material group, and often does so. For example, Bi_2Te_3 and Sb_2Te_3 have phase change and thermoelectric properties, and can also be characterized as topological insulators.

2.1 Phase change materials

The study of phase change materials began in the 1960s. In 1968, Stanford Ovshinsky proposed a group of materials that could be repeatably converted from a high resistivity state to a low resistivity state and back with the aid of an electric field. According to him, these materials would mainly be amorphous intrinsic semiconductors, such as oxygen- and boron-based glasses, and materials combining tellurium and arsenic with the elements from groups 13, 14 and 16. Ovshinsky also purported that with some compositions, the aforementioned low resistivity state would remain, even when the electric field is removed [2]. Even though the current phase change material compositions are discussed later, the last condition stated by Ovshinsky is

vitally important. Phase change materials are indeed non-volatile memory materials, meaning their information is not lost when electricity is no longer supplied.

There have been discussions on a universal memory that would be able to replace most currently used memory technologies [3]. In addition to the already mentioned non-volatility, this memory would need to pack large amounts of information into small spaces and store it for a long time. The read, write and erase operations should be very fast, repeatable and managed with little power. Finally, the whole construction should be inexpensive and compatible with silicon technology [3, 4]. Although these requirements may sometimes seem contradictory, they serve as a good basis, against which new accomplishments can be compared. The requirements also present clear goals to strive towards.

As with any memory, distinct states are required to keep the information. In the case of phase change materials, the zeros and ones for the memory devices are created by the amorphous and crystalline phases of the materials, and the changes from one phase to the other. Therefore, the material properties between the phases need to be different.

In general, although the amorphous phase does not have the long-range order of a crystal, a short-range order can exist. This means that some order can be detected at the nearest-neighbor and next-nearest-neighbor distances, like similar bond lengths, coordination numbers and bond angles [5].

Due to these structural differences, there are two distinct material properties of the phase change materials, which differ significantly from the amorphous to the crystalline state. Reflectance values are higher for the crystalline than the amorphous materials. The difference can be in the order of 20 % [6], depending on the alloy and wavelength [4]. The difference in resistivity between the phases is even greater, a phenomenon already presented by Ovshinsky. This difference is often several orders of magnitude.

Both of these differences in material properties are utilized in the memory devices. The reflectivity difference has been utilized in rewritable CDs and DVDs already for decades [4]. The more recent application of phase change random access memory uses the large difference in resistivity, possibly enabling even multilevel storage [7] and logic operations [8]. The phase change random access memories are already in production, in the 45 nm node [9], and used in mobile phones, such as the Nokia Asha [10].

The changes in phase are brought about by laser or electrical pulses. The detection of the amorphous or crystalline state is performed by a low intensity pulse that does not affect the material. The amorphous material is crystallized by a moderate power pulse, while amorphization is achieved by a shorter, more powerful pulse [11]. This is demonstrated in Figure 2.1. In general, the change in phase is caused by laser or current induced joule heating [9], though electronic excitations [12] might also have an influence. Phase change materials also exhibit a phenomenon called threshold switching [13], which allows for less power being used for crystallization [4]. When the phase change material is subjected to the threshold voltage or electric field, a fast electronic transition enables a larger current to pass through the still amorphous material which, in turn, heats the material and leads to its crystallization [4].

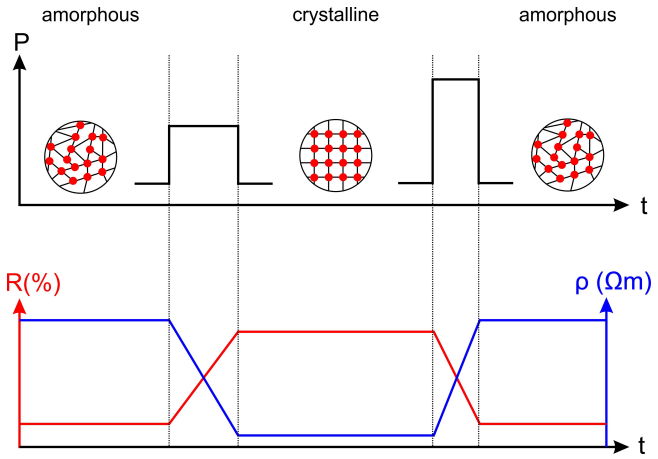

Figure 2.1: Differences in phase change material properties during crystallization and amorphization. P is the power of the laser/electrical pulse, R the reflectivity and ρ the resistivity of the material.

The crystallization in itself is a thermodynamically favored process. The kinetic hindrance to the crystallization, on the other hand, enables data-retention [9], which is a crucial property for memory applications. The required storage time is 10 years at 100 or even at 150 °C, if automotive applications are considered [11].

The quick crystallization is caused by the poor glass-forming properties of the phase change materials. Glass-formers are inorganic substances that do not crystallize during melt-quenching, but solidify as an amorphous phase. The glassy states have higher energy, entropy and volume than their crystalline counterparts. Moreover, since good glasses do not crystallize easily [12], poor glasses are thus needed.

Interestingly, the time needed for the crystallization is not constant. The initial crystallization of the amorphous material is the slowest process [11]. When this material, or parts of it, are first melt-quenched back to the amorphous phase and then recrystallized, this second and further

crystallizations progress much faster than the initial crystallization [14]. This can be explained, for example, with the recrystallization starting from the interface with the surrounding crystalline material. Crystallization can thus occur without additional nucleation [15]. In addition, the melt-quenched amorphous material can have much more medium range order than the as-deposited amorphous material, making the recrystallization faster [16]. The recrystallization process can occur even in less than 1 ns [17].

The faster recrystallization is especially true for the growth-dominated materials, where most of the crystallization occurs via growing nuclei. The additional order also helps with nucleation-dominant materials, where the crystalline volume grows mainly by newly forming nuclei [18, 19].

Some examples of phase change memory devices are presented in Figure 2.2. The first example is an optical memory device in Figure 2.2a. The phase change material is only one of the layers in the multilayer stack consisting, for example, of dielectric $ZnS-SiO_2$, reflective Al and the polycarbonate substrate [20]. The most simple electrical device structure is the so-called mushroom cell in Figure 2.2b, where the phase change material is sandwiched between the top and bottom electrodes and heaters. The crystallized region forms into the horizontal phase change structure right above the heater. While this type of structure is good for testing, it does not enable sufficient scaling. With scaling, also the reduction of the reset current is desired [21]. This could be achieved by decreasing the contact area between the phase change material and the heater [22]. Overall, in more complex structures, the phase change material is no longer as a two dimensional layer, but confined into a trench [22] or a pore [23] such as in Figure 2.2c. These confined structures also result in better thermal insulation from neighboring structures. Such complicated structures and shrinking devices require specialized thin film deposition methods.

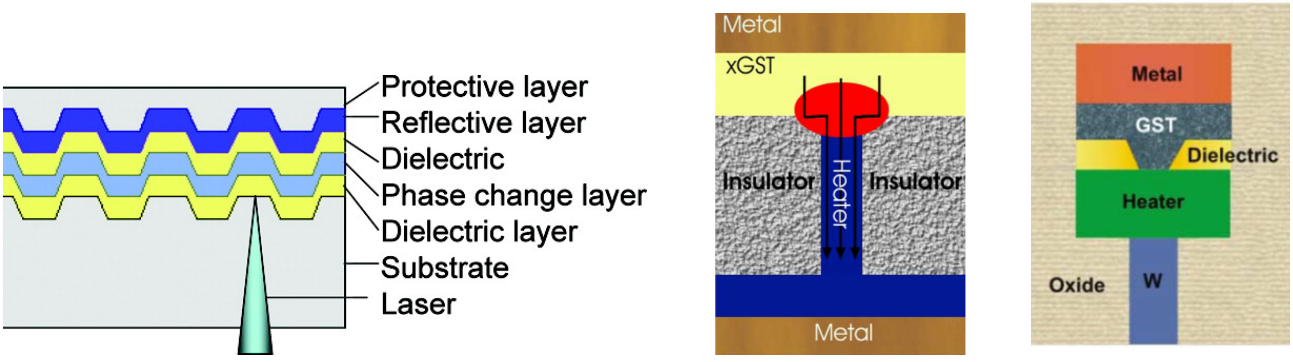

(a) (b) (c)

Figure 2.2: Examples of typical phase change memory device structures. Single layer rewritable DVD (a) and phase change random access memory configurations (b), (c). (a) Reprinted with permission from [15]. Copyright (2010) American Chemical Society. (b) and (c) Reprinted (adapted) from [24] with permission from Elsevier, Copyright (2006).

Once the device is in operation, it needs to endure the rewriting process and be reversibly switchable. To compete with dynamic random access memory (DRAM), $10^{16} - 10^{18}$ cycles are required. Currently, at least 10^{11} cycles have been proven [9].

Most of the materials studied today are in the ternary composition range of Ge-Sb-Te (GST), demonstrated in Figure 2.3, along with their common applications. The binaries GeTe and Sb_2Te_3 mix well and form a GST alloy. Numerous studies have been made on the compositions that lie in the tie-line between GeTe and Sb_2Te_3, making $Ge_2Sb_2Te_5$ the "classical" phase change material. The material composition can be varied since the GST alloys have stable compositions along the whole tie-line. Another important family of phase change materials is the Ag and In doped Sb_2Te, or AIST, family. In addition, Ge-doped Sb has proven to have phase change properties. Overall compositions in these alloys are tailorable to specific applications [4].

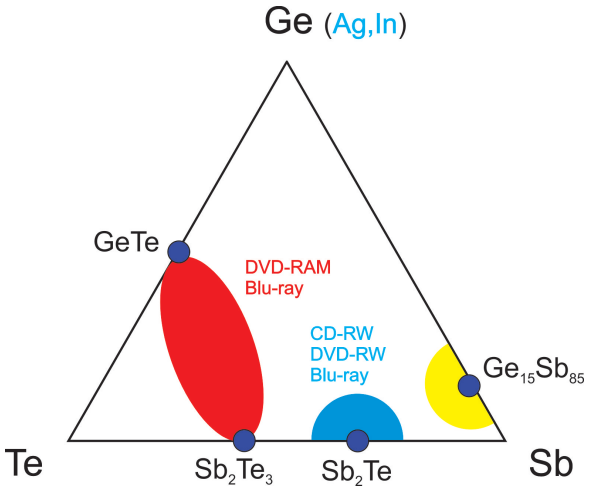

Figure 2.3: Phase diagram of phase change materials.

When choosing the right composition, also the crystallization properties need to be taken into account. The AIST family crystallization is growth dominated, while that of the GST family is nucleation controlled [18, 19].

Good reflectance properties at desired wavelengths are needed from materials in optical applications. Therefore, as an example, with changes in the laser wavelengths from IR to red and further to blue, compositions in the GeTe-Sb_2Te_3 tie line moved towards GeTe, as they have a higher contrast in the shorter wavelength, i.e. blue, region of the visible spectrum [4]. The changes in optical properties enable compositional tailoring for a specific application.

There have been great difficulties in determining the exact difference in structure between the amorphous and crystalline phases. The crystalline structure is naturally easier to determine, for example with x-ray diffraction (XRD). An amorphous material, by definition, does not have long range order. In the case of phase change materials, however, there have been indications of short range order with neighboring atoms, similar to crystalline materials. Pathways, such as the "umbrella-flip" of the germanium atom between a tetrahedral coordination in the amorphous state and an octahedral coordination in the crystalline state, have been suggested for the phase transition [25]. Nevertheless, it seems that Ge atoms in amorphous form also have mostly octahedral coordination. Therefore, it could be stated that similar bonding conditions exist in both forms, and the transitions within the structure are quite minor [26].

There are some factors that the crystalline structures of phase change materials have in common. These could be used as a basis for finding new materials that fit into this category. Phase change materials exhibit resonant bonding. As an example, Sb has three valence p-electrons to form orthogonal bonds. In its crystalline structure, Sb has six roughly equivalent nearest-neighbors to form bonds with, giving rise to two limiting possibilities of bond structures. Simplified versions of this are presented on the left and right sides of Figure 2.4. In reality, the hybrid form of these exists (Fig. 2.4, middle), making the bond structure resonant, even with some Peierls distortions in the crystal structure [27]. Overall, the hybridized structures are fairly symmetric, or close to the octahedral-like coordination [28]. The resonance bonding is not present in the amorphous phase, thus presenting one reason for the large contrast in electrical properties between the phases [26].

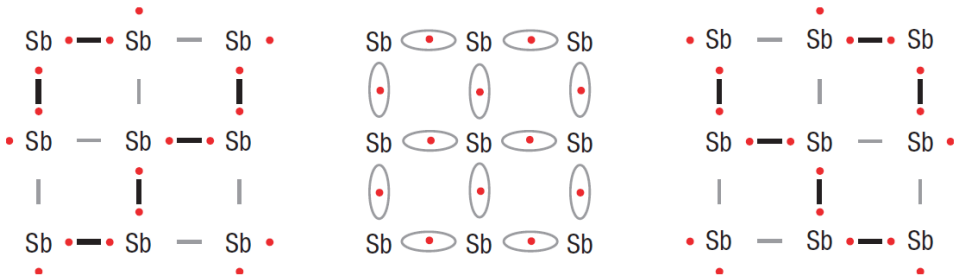

Figure 2.4: Simplified resonance structure of Sb, with the extremes on the sides and the hybrid structure in the middle. Reprinted by permission from Macmillan Publishers Ltd [27], Copyright (2008).

In many of the phase change materials, these same three p-electrons per atom are present. When we also take into account the ionicity of the bonds, denoted by the difference in valence radii of the p-orbitals [28], a plot such as Figure 2.5 [26] can be made. It is abundantly clear that all known phase change materials are located in a very small area of the diagram, indicating that a very specific bonding character is needed. A curious outcome of this type of plot of

chalcogenide materials is the overlap of the material classes. The same combination of ionicity and hybridization of phase change materials is also found in known thermoelectic materials and topological insulators. These types of theoretical studies are important as they open whole new possibilities in using the materials at hand, and provides a good tool for discovering new materials within the desired property ranges.

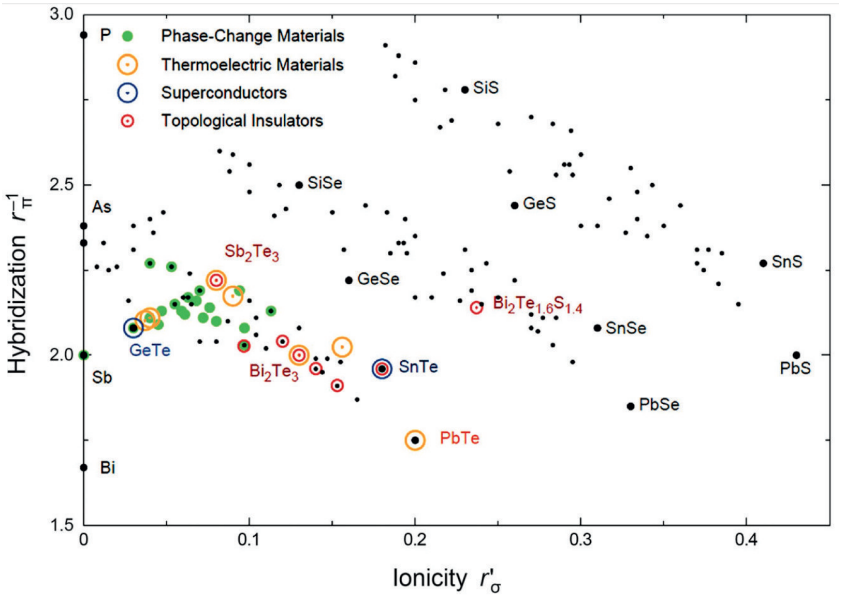

Figure 2.5: Map of materials with, on average, three p-electrons per site. Reprinted with permission from [26], Copyright (2012) John Wiley and Sons.

In general, phase change materials can be made by both physical vapor deposition (PVD) and chemical vapor deposition (CVD) methods. In addition, chemical synthesis of nanoparticles is also an option [29, 30]. Thin films of change materials are mostly made by sputtering, against which all the other methods, and the material properties produced by them, can be compared.

All PVD methods use high or ultra high vacuum (UHV) conditions. In PVD, material is removed from a solid source or target by supplying energy in the form of heat, molecular bombardment or a laser beam. Atoms or molecules traverse in direct paths through the vacuum to the substrate. These direct paths of the atoms make PVD a line-of-sight method, meaning that only the top surface of the substrates can be coated. In addition to sputtering, phase change materials have been made by simple evaporation [31, 32], pulsed laser ablation (PLA) [33, 34], molecular beam epitaxy (MBE) [35, 36]. Nanowires [37] have been made using the vapor-liquid-solid (VLS) [38] method, along with nanoparticles created by PLA [39, 40].

CVD methods utilize chemical reactions to form the products. In a typical process, gaseous precursors are brought into the reaction chamber and to the substrate surface, where they adsorb and react, forming the desired end product along with a number of volatile side products [41]. Often these precursors are metal-organic, making MOCVD (metal-organic CVD) the most common type of CVD. Unlike in PVD, CVD processes enable depositions on three dimensional substrates. Phase change materials have been deposited by both thermal CVD [42–45] and by plasma-assisted CVD [46, 47].

2.2 Thermoelectric materials

The thermoelectric phenomenon is mainly based on two effects. According to the Seebeck effect, a temperature gradient across a material or a device produces a voltage. The complementing Peltier effect causes a temperature difference across a material or a device when a current is passed through it [48, 49]. Examples of the devices are depicted in Figure 2.6. The devices are connected electrically in series with conducting strips. Thermal conduction is ensured with electrically insulating but thermally conducting plates to connect the separate p/n-pairs, i.e. the legs, into a module [49].

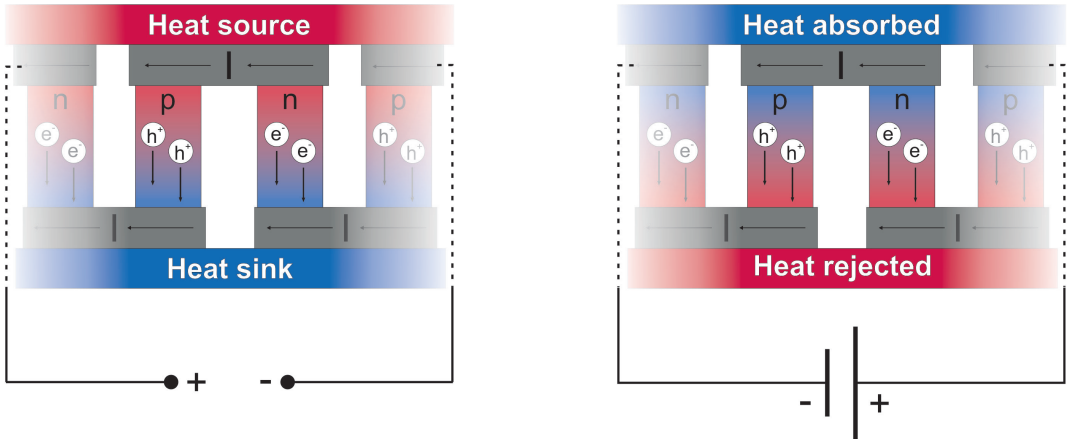

(a) (b)

Figure 2.6: Schematics of a Seebeck device (a) and a Peltier device (b).

In general, thermoelectric materials have a high specific power (watts per volume or mass), which enables scaling to low power levels. They are very useful in applications where low weight and small size are more essential than the production costs. In addition, thermoelectric devices have no moving parts and thus need no maintenance, which makes decade-long operation possible.

The Seebeck effect is used in thermoelectric power generation, such as on the Apollo Lunar missions, Voyager space probes, and in many hard-to-access locations on Earth where constant power and low maintenance are required [49]. The same effect can also be utilized in waste heat utilization, in factories for example. The Peltier effect is used in cooling applications, be it a simple USB-plugged beverage container [50], a car-seat temperature-control system [51], or more sophisticated devices such as lasers and infra-red sensors [52, 53].

The efficiency of thermoelectric materials is usually determined by a dimensionless figure of merit, ZT (Equation 2.1), where S is the Seebeck coefficient, σ is the electrical conductivity, κ is the thermal conductivity and T is the absolute temperature. Therefore, a good thermoelectric material or device needs to have a high Seebeck coefficient to achieve a larger voltage, a high electrical conductivity to minimize the parasitic or joule heating of the cold side, and a low thermal conductivity to maintain the temperature difference as high as possible [54].

$$ZT = \frac{S^2\sigma}{\kappa}T \tag{2.1}$$

The difficulty lies in fulfilling these seemingly simple terms in the same material. Although there is no fundamental upper limit for ZT [49], there is interdependency between the factors affecting ZT through the electronic properties of the material. When the Seebeck coefficient increases, the electrical conductivity decreases due to carrier density effects. Moreover, when the electrical conductivity increases, thermal conductivity increases as well due to the Wiedemann-Franz law [55]. This can make it difficult to achieve ZT values greater than 1 in bulk or 3D materials [55, 56]. In addition, the thermal conductivity κ consists of electronic and phononic components, which is demonstrated in Equation 2.2.

$$\kappa = \kappa_e + \kappa_p \tag{2.2}$$

The focus is often at decreasing the phononic component of the thermal conductivity as the the electronic component is related to the electric conductivity according to the Wiedemann-Franz law [55, 57]. The more the lattice vibrations can be disturbed, the better. An all-encompassing approach has been proposed to achieve all this. The aim is a phonon-glass electron-crystal (PGEC) structure: the electronic properties of a crystalline solid (high S and σ), where the electron mean free paths are long, and the thermal properties of a glass (low κ_p), where the

phonon mean free path is short. These materials could be found amongst heavy-element compound semiconductors that have small band gaps and complex crystal structures [58].

Up until the 1990s, thermoelectric materials were made mainly in bulk form, and their ZT values were at the highest close to unity [52, 59]. A new possible approach was discovered in 1993 [60, 61], suggesting that significant increases in ZT values were possible by using nanostructured materials. This enabled engineering thermoelectric materials from the start, not just using the natural materials available. The so-called second generation materials were already able to achieve $ZT = 1.3 - 1.7$ by decreasing the lattice thermal conductivity by using mixed compositions and nanoscale precipitates. The current third generation materials are reaching values of $ZT = 1.8 - 2.2$ by optimizing band structures and suppressing phonons on all length scales [62]. Nanostructuring the devices gives an opening for thin film deposition methods, such as ALD. General trends in ZT values for different materials can be found in Figure 2.7.

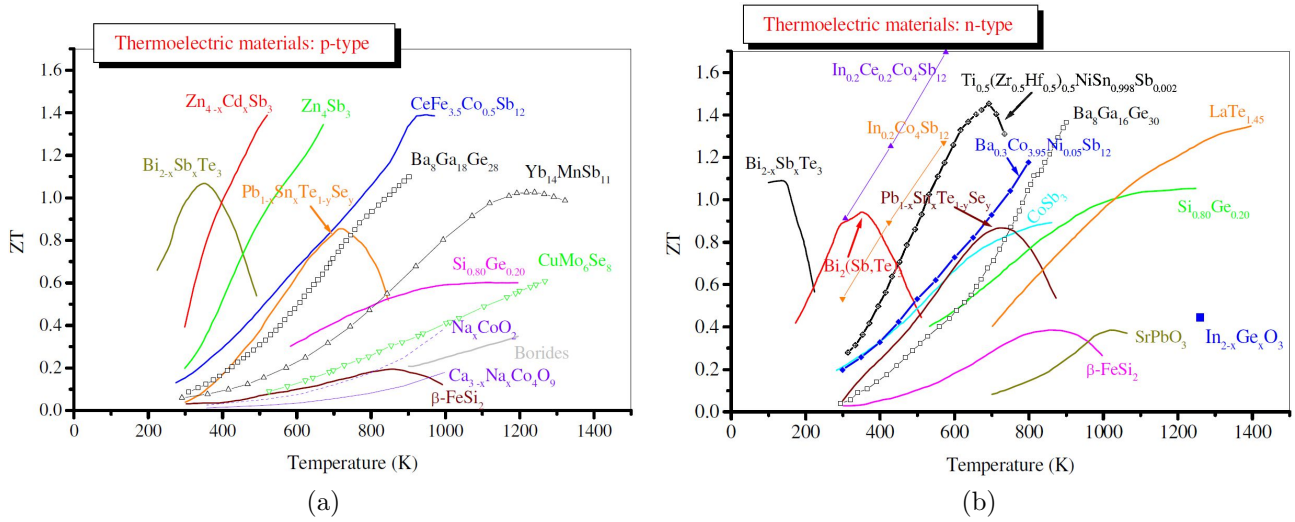

Figure 2.7: ZT values of p-type (a) and n-type (b) materials in terms of absolute temperature T. Reprinted (adapted) with permission from [63], Copyright (2009) Cambridge University Press.

The nanostructuring can be done in different length scales, since the lattice vibrations, i.e. phonons, have different wavelengths or mean free paths. Complex crystal structures increase the number of phonon modes. Each of the phonon modes can then be handled separately. The shortest wavelength phonons are scattered by the shortest length scale defects, such as point defects and dopant atoms on lattice sites. These include both vacancies and mass contrast caused by heavier or lighter dopant atoms. For example, heavy atoms within the structure, such as within voids, can vibrate independently causing disturbances in the phonon propagation. The medium wavelength phonons can be scattered by basic nanostructuring, such as the interfaces between the matrix and the precipitate. Mass contrast can also be created between the different

phases. The long wavelength phonons are accordingly scattered by the largest scale defects in the material. This can be achieved via grain boundaries by breaking down the crystals to the mesoscopic scale (100 nm - 5 μm). Finally, the material can be sintered back into a bulk object [62, 64].

Nanostructuring can be combined simultaneously with hierarchical architecture, band alignment and other electrical structure engineering. Zhao *et al.* [62] called this all-encompassing engineering the "panoscopic approach". The band engineering is performed by having the valence and conduction band energies of the two or more phases close to each other to ensure good transport properties.

Thermoelectric materials include a myriad of materials, only some of which are mentioned here. Those known for decades are Bi_2Te_3, PbTe and SiGe alloys. They are used at low, intermediate and high temperatures, respectively, due to the varying temperature dependence of their ZT values. It needs to be taken into account, however, that all the mentioned thermoelectric materials are doped to optimize their properties, even if not always explicitly noted.

The bismuth telluride alloys have their maximum ZT levels a little above room temperature, at about $350 - 450$ K. Bi_2Te_3 and its alloys are therefore the main sources for refridgeration and also energy generation at low temperatures. Sb_2Te_3 is often alloyed with Bi_2Te_3 to increase ZT by decrasing thermal conductivity and leaving the electronic properties mostly unchanged. This type of an alloy leads to a p-type composition, often near $(Sb_{0.8}Bi_{0.2})_2Te_3$. In a similar fashion, an n-type alloy is formed by alloying Bi_2Te_3 with Bi_2Se_3, to compositions such as $Bi_2(Te_{0.8}Se_{0.2})_3$ [49, 57, 65].

Lead telluride and its alloys were one of the first thermoelectric materials discovered. They have a cubic NaCl-type crystal structure and excellent thermoelectric properties. They are generally used in the temperature range of $500 - 900$ K, where intrinsic ZT values as high as 1.4 can be reached. A PbTe−PbSe has even achieved $ZT = 1.8$. Lead tellurides, or selenides, are also doped, often with halides and alkali metals. Further ZT improvement can probably be achieved through nanostructuring [66]. Good performance has also been found in materials similar to lead tellurides, such as the TAGS, $(AgSbTe_2)_{1-x}(GeTe)_x$, or LAST, $(AgSbTe_2)_x(PbTe)_{1-x}$, where values of $ZT > 1.5$ can be reached [49, 57, 67].

The complete miscibility of Si and Ge ensures a large variety of possible alloys such as the common $Si_{0.8}Ge_{0.2}$. Although the miscibility is good, care needs to be taken during preparation, as Si- and Ge-rich regions form easily. The SiGe alloys work best at very high temperatures, around $900 - 1300$ K, although they can be operated at much lower temperatures as well. A

wide temperature range can mean very efficient operation. For thermoelectric devices, the SiGe alloys are doped with boron for p-type and phosphorous for n-type materials [68].

The demands for higher ZT values and the onset of multileveled approaches to nanostructuring have brought along several new materials classes into the family of thermoelectrics. Many of these are also chalcogenides and pnictides. In general, the recent additions to thermoelectrics strive for PGEC properties with complex crystalline structures.

Half-Heuslers are a group of semiconducting materials made of metallic elements. The XYZ composition is made of an electropositive metal X (Ti, Zr, Hf), a late transition metal Y (Co, Ni) and a main group element Z (Sn, Sb). The crystal structure can be thought as an fcc Z lattice, with metal X in the octahedral holes and metal Y in half of the tetrahedral holes, leading to an XZ rocksalt sublattice and a YZ zincblende sublattice. In general, these half-Heusler materials have large power factors ($S^2\sigma$), although combined with a large κ. By including several of the possible metals in the same structure, point defects can be formed, leading to a decrease in κ. Therefore, ZT values of ≥ 1 have been achieved at temperatures above 750 K, when practically all the aforementioned metals were used together in an n-type composition [56].

Skutterudites are a class of compounds with a $CoAs_3$ type structure. They can be generalized with the formula MX_3, where M is a transition metal (Co, Rh, Ir) and X is the pnictogen (P, As, Sb). Skutterudites have an open body-central-cubic crystal structure, with a void in the center of the unit cell. The pnictogens form planar σ-bonded rings within the structure. The binary skutterudites have high mobilities but also a high thermal conductivity, which makes them unsuitable for thermoelectrics as such. When the structural void is filled with atoms with a large mass and a small diameter, such as rare-earth or alkaline-earth metals, the thermal conductivity is reduced and thermoelectric applicability is achieved. Not all voids need to be filled and can be filled with different elements at the same time. Depending on the inserted atoms, both p- and n-type materials can be achieved. The inserted elements cause a rattling effect, where the heavy atom vibrates independently from the rest of the crystal structure, which significantly decreases thermal conductivity, enabling ZT values of over 1.5 in the range of $700 - 1000$ K [53, 69, 70].

Zintl compounds are represented with the nominal formula AM_2X_2, where A is an alkaline-earth or rare-earth metal, M is a transition metal or a main group metal, and X is an element from groups 14 and 15. They are usually air sensitive, with a complex crystalline structure such as $ThCr_2Si_2$. The large unit cell and the combination of covalent and ionic bonds fulfill the PGEC criteria of low thermal and high electrical conductivity. [53, 57]

There are still several other material groups that have thermoelectric properties and do not contain chalcogen or pnictogen elements. Oxides, such as cobaltites and perovskites are studied because they are chemically and thermally stable even in high temperature gradient conditions and in air. In addition, they can be easily chemically modified and compositionally tailored. Low costs and environmental friendliness are also desirable properties. At best, oxides have reached ZT values of 0.65 [71]. Another group of inorganic materials that has demonstrated thermoelectric properties is metal silicides, which can be used at high temperatures. The best ZT values around unity have been achieved with magnesium and manganese silicides [49, 68].

All the above described materials are inorganic. Nevertheless, organic materials have been proven to have thermoelectric properties as well. They would be an alternative to the inorganic materials due to elemental abundance, low cost, chemical modifiability and mechanical flexibility. Organic thermoelectric materials are mainly conducting π-conjugated polymers such as polyaniline and polyacetylene. Their low intrinsic ZT values have been sometimes compensated with hybrid structures with more familiar inorganic thermoelectric materials. Overall, a good deal of work is still to be done here. Especially the thermal stability is an issue, as polymers do not withstand high temperatures [72].

Thermoelectric materials are a varied group and cannot be categorized simply. They contain many elements in increasingly complex structures. Material structure engineering has led to various compounds having ZT values in excess of their bulk values presented previously, as can be seen in Figure 2.8. Nevertheless, high ZT values do not lead to an instant success in real world applications. To achieve more than a niche market, mass production is needed, where cost is always an issue. Therefore, with elements like antimony, the noble metals and the rare earths, there can be a market risk of increasing costs due to scarcity and a small number of production sites. Thus, thermoelectric materials need to be evaluated not only on their properties but also on their applicability to production [73].

Actual thermoelectric devices, especially the legs (see Figure 2.6) made of the n- and p-type thermoelectric materials, are still macroscopic in size to accommodate large temperature differences across the devices. Therefore, also the methods to manufacture these materials are bulk methods.

The initial thermoelectric material is often made with powder metallurgical tehniques or by mechanical alloying [49]. Other possibilities include melt-spinning [64] or melting from elements [74].

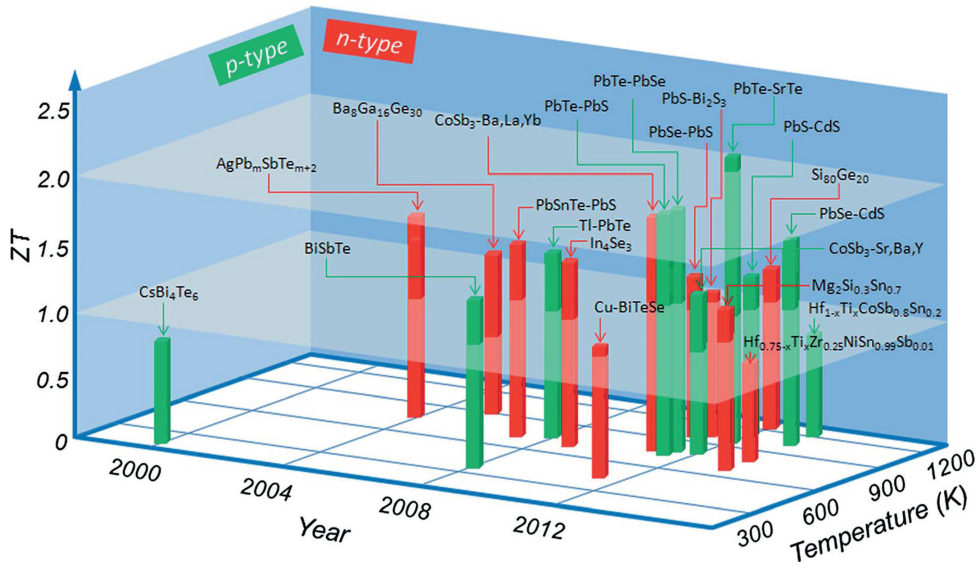

Figure 2.8: State-of-the-art ZT values for different materials. Reproduced from [62] with permission from The Royal Society of Chemistry, Copyright (2014).

Since nanostructuring is practically a requirement these days, the starting material can also be made in the form of nanoparticles. These can be made via wet chemical methods, hydrothermal growth or inert-gas condensation [53]. If the thermoelectric material is made in bulk form, it is usually ball-milled into an appropriate grain size.

When the thermoelectric material is in a powder form, it needs to be compacted into the final form of a leg in a device, or part thereof. The compacting of the powders is often achieved via sintering methods, such as spark plasma sintering and current-assisted sintering [64]. Other compacting methods include wet chemical methods, hydrothermal growth, and inert-gas condensation [53]

As all of the thermoelectric materials have their optimal temperature ranges where they perform the best, segmenting has become a tool. Several thermoelectric materials can be combined in the segments of a device leg so that each one is functioning in its optimum temperature range [57]. As these segments need to be bonded together, the preparation methods need to be well chosen to achieve a good contact between the materials.

2.3 Topological insulators

Topological insulators are a curious group within the chalcogenide materials. Their existence was theorized a number of years ago [75], after which they gained great scientific interest. The theoretical predictions were confirmed with experimentally measured results very soon afterwards [76, 77].

As the name implies, topological insulators are insulating in the bulk. The intriguing properties arise from the surface, where metallic conducting states can be found. This is made possible by the time-reversal symmetry of the conducting states [78–80], which is typical for heavier elements [79–81].

It appears that topological insulators are mostly chalcogenides with layered crystal structures. For example, several of the proven compounds, such as Sb_2Te_3 [78], Bi_2Te_3 [82] and Bi_2Se_3 [77] all have the same crystal structure.

Spintronics and quantum computing have been envisioned as possible applications for the topological insulators [82, 83]. This again implies that the materials need to made in non-bulk form. A good way to make a surface-reliant material would be a surface-controlled method such as ALD.

2.4 III-V semiconductors

As the name implies, III-V semiconductors are comprised from the elements of groups 13 (III) and 15 (V). Examples of these compounds are GaAs and InP. Not naturally occurring, this category of materials became an intense subject of study already in the 1950s [84, 85]. After this, their interesting electric properties were enough to fuel the research efforts.

Many III-V compounds have their band gaps close to the visible range, making them ideal candidates for optical applications. As an example, one of the most studied III-V compounds, GaAs, has a direct band gap of 1.4 eV, which puts it in the infrared region, while the band gaps of others such as AlN are in the ultraviolet region [86]. Many industrially important III-V semiconductors are ternaries or even quaternaries, such as $Al_xGa_{1-x}N$ and $Al_xGa_yIn_{1-x-y}As$, which means their properties, like band gaps, can be adjusted by compositional variations. Consequently, tailor-made materials can be made for the applications [87].

It is the direct band gap that enables an efficient radiative recombination of electrons and holes, which leads to photon emission. A very simple LED can be achieved with a p-n junction in GaAs [88, 89]. When the alloys mentioned above are combined in multilayer stacks or quantum wells and other complicated structures, a wide range of wavelengths can be covered [87]. The blue LEDs based on GaN [90] have been the latest addition to LED wavelengths, thus giving rise to significantly more research on white LEDs, for example. The same III-V direct band gaps and optical properties derived thereof, also enable lasers [91–93] with similar heterostructures and quantum wells. Another optoelectronic application of III-V compounds is solar cells [94].

Due to the high carrier mobility, compared to Si in particular, GaAs has been an attractive candidate for microelectronics, as transistors could be made to work faster this way [95]. InAs has an even higher electron velocity [87]. The special band structure of GaAs enables negative resistance effects [96, 97], which can be utilized in microwave production such as in a Gunn diode [87, 98]. Electronic components usually require heterostructures, which can be easily formed as GaAs has a small lattice mismatch with many of its alloys [87].

As III-V compounds are needed for their electrical properties, low impurity levels are crucial. Therefore, single crystal methods have been popular for making them. Single crystals can be grown, for example, with the liquid encapsulated Czochralski [99, 100] and different Bridgman and gradient freeze methods [101–103].

In optoelectronics applications, thin films are also needed. These can be made, for example, with liquid phase epitaxy [87, 104]. In addition, there are physical vapor deposition methods such as evaporation [105] and molecular beam epitaxy [104, 106, 107]. Chemical vapor deposition (CVD) methods include metal-organic CVD (MOCVD) [108], also known as metal-organic vapor phase epitaxy (MOVPE), and atomic layer epitaxy (ALE) [109–111].

Generally, III-V thin films have been deposited on III-V substrates, either on the same material or on something with a small lattice mismatch. Compositionally different materials, such as sapphire and silicon, have also been used as the interface layer is important for high crystal quality. Overall, the deposition temperatures have been relatively high, in the $400 - 700\,^{\circ}\mathrm{C}$ range. Some materials, such as GaN, require even higher temperatures of over $1000\,^{\circ}\mathrm{C}$ [87].

Chapter 3

Atomic layer deposition of chalcogenides and pnictides

Atomic layer deposition was initially developed for depositing thin, pinhole-free, conformal films for thin film electroluminescent displays (TFEL). The first process was also a chalcogenide, the phosphor material in TFELs, ZnS:Mn [112]. Soon thereafter, another ALD process for a chalcogenide, this time ZnTe, was presented [113]. Since that, ALD has proven itself in many different nanotechnological applications such as microelectronics [114].

Although TFELs are still in production, the main applications of ALD these days are in the semiconductor industry. High-k materials are needed in MOSFET and DRAM device structures as well as in double-patterning lithography. Other applications include the magnetic read/write heads for hard disks and protective coatings for silver jewelry to prevent tarnishing during storage [115].

The reason for taking ALD into use in microelectronics and many other applications is the miniaturization of devices, which increased the requirements for deposition controllability. Miniaturization has also led to increasingly complex three-dimensional devices such as tri-gate and FinFET transistors. For most PVD methods, thin film deposition outside line-of-sight is difficult. Therefore, chemical methods, such as ALD, are needed for conformal, repeatable, and good quality film deposition.

A large number of materials have been deposited by ALD during the 40 years the method has been used [116]. Both chalcogenides and pnictides have been the focus of intense study, and thus several chemistries have been used to deposit these thin films, both epitaxially and non-epitaxially.

3.1 Principles of atomic layer deposition

Atomic layer deposition (ALD) is a gas phase thin film deposition method, a modification of chemical vapor deposition (CVD). Unlike in CVD where precursors can react already in the gas phase before reaching the substrate, in ALD the precursors are brought to the substrate one at a time. A simple ALD cycle is demonstrated in Figure 3.1.

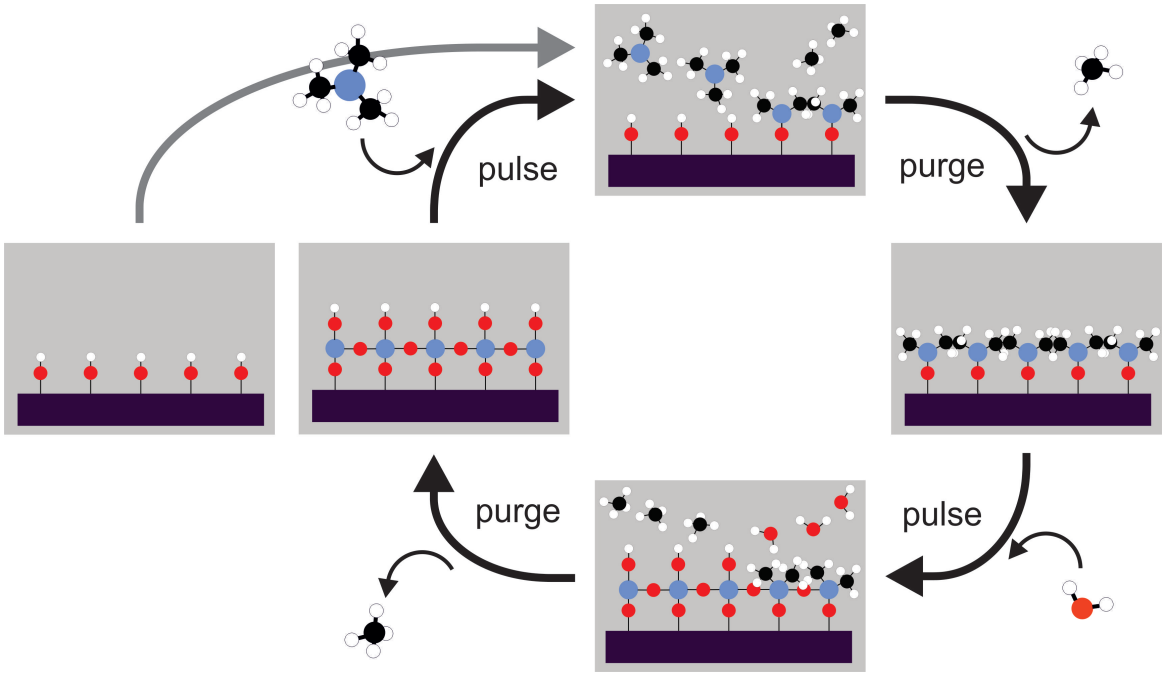

Figure 3.1: Representation of an ALD cycle.

The precursor molecules react with surface groups until all available sites are occupied, making ALD a saturative method. It is thus self-limiting, as growth stops when all the surface groups have reacted. A purge separates the precursors from each other in space or in time, removing excess precursor molecules and reaction byproducts. The second precursor can then be brought to the substrate surface where a new set of saturative reactions occur. Another purge completes the basic ALD cycle.

When each ALD cycle deposits the same amount of material - a fraction of or a full monolayer of film - the desired film thickness can be achieved simply by controlling the number of deposition cycles. The saturative reactions enable uniform thin film deposition on even the most demanding three-dimensional and large area substrates [117, 118].

Generally, ALD processes are not strongly temperature dependent. There can be a wide "ALD window", where the growth rate stays fairly constant [116]. Some temperature variations in growth are shown in Figure 3.2. Part 3 represents the stable ALD window, which does or does

not exist for a process. A process can still have all the typical ALD characteristics, even if there is no ALD window. In part 3A, the growth rate is temperature independent, while in 3B the growth rate is temperature dependent. This difference can be caused by a possible temperature dependence of the density of the reactive sites [117].

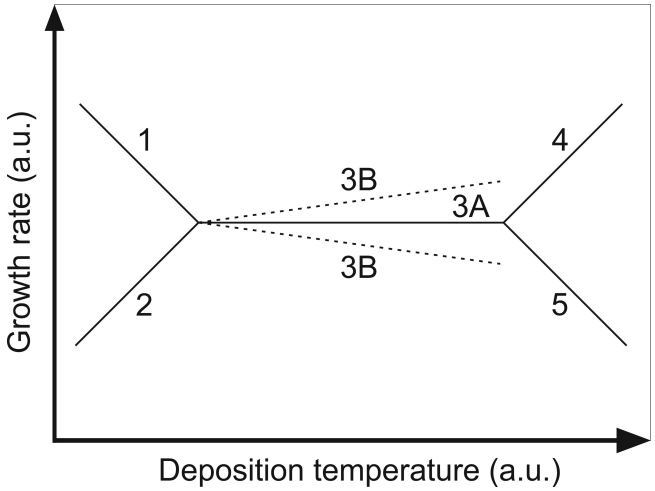

Figure 3.2: ALD process properties with respect to the deposition temperature.

The increase in growth rate in part 1 can be due to multilayer adsorption of the precursors or condensation of low vapor-pressure precursors. The effect becomes more prominent with decreasing temperatures, because the volatility continues to decrease. In part 2, the growth rate decreases with decreasing temperature. This might be due to kinetics slowing down the reactions so that they are not completed. With the temperature increase, the system has more energy, which can speed up the reactions towards completion [117].

The growth rate increase in part 4 means that the self-limiting conditions no longer apply due to precursor decomposition. This causes more reacting species to be involved in the growth reactions. These unwanted species might interfere with the intended process by competing or additional reactions. The self-limiting conditions can be lost also due to precursor desorption, which causes the growth rate decrease in part 5. If the precursor no longer sticks to the surface, less reactions occur and less material is deposited [117].

This basic form of ALD is also called thermal ALD, since the activation of the chemical reactions is achieved through heat. Other forms, usually with lower deposition temperatures, utilize plasma (plasma-enhanced ALD, PE-ALD) [119] or light (photo-assisted ALD) [120] as sources of energy. The energetic species created by the plasma, such as ions or radicals, add energy to the system [121]. Recent developments in ALD, and especially in reactor design, have added some old and new variations to the method. Spatial ALD, where the precursors are separated in space and the substrate moved between them, has made a return into the ALD toolbox,

having been the initial concept in Suntola's work [112]. Spatial ALD has been developed so far now that some robust ALD processes are used to deposit thin films on very long substrate surfaces traveling from roll-to-roll [115].

For any ALD process to work properly, certain important properties are required from the precursors. The most obvious property is sufficient volatility, as ALD is a gas phase method. The precursor should have a vapor pressure of $0.1 - 1$ mbar [115] at a reasonable temperature below the deposition temperature so that condensation before reaching the substrate is avoided. Next, the precursor needs to be highly reactive with its counterpart, yet not reactive enough to etch or otherwise destroy the growing film and the reactor parts. The byproducts also need to be volatile to be easily removed by the purge. In addition, as thermal stability is needed, the precursor should not decompose at the deposition temperature. [115–117]

Several other factors should also be taken into account when considering precursors. Toxicity to the user is one issue. Many precursors are relatively safe to handle with minor precautions, yet some require special attention [115, 117]. For example, H_2O is perfectly safe, and H_2S can be used rather safely from an external gas bottle even in a regular laboratory. Nevertheless, any gaseous pressurized precursors need to be handled carefully. When progressing down in the periodic table, H_2Se and H_2Te are very toxic already in small concentrations where they cannot be smelled, unlike H_2S. Therefore many more precautions would be needed to use these precursors [122].

Environmental friendliness is another issue, as waste is always created during an ALD process, particularly through the unreacted precursors and byproducts that are purged away during a deposition cycle. One consideration is cost. While in the scale of research laboratories, proof-of-concept studies can be made with very little precursor, industrial applications might not be feasible due to costs. [115–117]

ALD precursors encompass a wide variety of different types of compounds. Metal precursors are usually inorganic, metalorganic or organometallic. Inorganic precursors are simple - either elements themselves or halides. Common metalorganic precursors can be organometallic and have direct carbon-metal bonds with ligands, such as alkyls and cyclopentadienyls, or they can be plain metalorganic and have ligands bonded through a non-carbon such as alkoxides, β-diketonates, amides, imides, amidinates and phosphines. The most common non-metal precursors are hydrides such as H_2O and NH_3 [115–117].

3.2 Atomic layer deposition of chalcogenides and pnictides

The assortment of ALD processes has been growing ever since the early days of Suntola. Both scientific curiosity and the needs coming from industrial applications have driven the research. Nevertheless, a number of potentially industrially relevant chalcogenide and pnictide materials did not have ALD processes as little as a decade ago. This group included the already mentioned material categories of phase change materials and thermoelectric materials.

3.2.1 Chalcogenides

Zinc sulfide was one of the early ALD success stories, and there is a substantial list of sulfides already made by ALD [116]. Most of the reported sulfide materials can be made by combining a metal halide [123–126] or a metal-thd (thd = 2,2,6,6-tetramethyl-3,5-heptanedione) complex [123, 127, 128], with H_2S, the most common sulfur precursor. In some cases, such as ZnS [112, 129] and CdS [130, 131], the elements can be used for the metal and non-metal precursors.

Only two selenide materials, ZnSe and CdSe, have been reported prior to introducing alkylsilyls selenides as precursors. Nevertheless, there are a number of different processes reported for ZnSe and CdSe. As with the sulfides, elements can be used to form both selenides [131–134].

There were few reports of telluride ALD until the recent alkylsilyl-enabled processes. The simplest of these processes used the respective elements as precursors, for example in MgTe [135, 136], MnTe [136–139], ZnTe [132, 138] and CdTe [131, 136–139].

When elements cannot be used for depositing selenides, H_2Se becomes the precursor of choice. It is most often combined with a zinc alkyl, either dimethyl [140, 141] or diethyl zinc [142], although ZnSe can also be deposited from elemental Zn and H_2Se [143]. Both dimethyl zinc - H_2Se processes used low deposition temperatures, with the ALD window at around 150 °C, and growth rates saturating to 1 ML/cycle. The diethyl zinc - H_2Se process, or a silylamido zinc - H_2Se process, needed deposition temperatures a few hundred degrees higher [142]. Similarly, the use of *in situ* created $ZnCl_2$ as the zinc precursor led to high deposition temperatures, with the ALD window as high as $400 - 500$ °C. All of these processes used H_2 as the carrier and purge gas. There has been only one instance where CdSe was mentioned being prepared from non-elemental sources, by combining dimethyl cadmium with H_2Se [144].

Differently from the selenides, alkyl tellurides have been utilized in most of the reported ALD telluride processes. On each instance these have been combined with alkyl compounds of the metals. Also with tellurides, the carrier and purge gas used was H_2. The most common telluride material to be produced is CdTe, while HgTe [145, 146] and ZnTe [147] are barely mentioned. To deposit CdTe, Me_2Cd is combined with $^{i}Pr_2Te$ [148, 149], Et_2Te [147, 150] or MeAyTe [145, 147, 150], where Ay is the allyl ligand. Most CdTe processes have their optimum deposition temperatures around 300 °C, while the growth rates saturate to 1 ML/cycle.

3.2.2 Pnictides

Pnictides, and especially the III-V semiconductors have been industrially important materials for several decades already. The nitrides are the most abundant group of ALD pnictide processes. In nitride thermal ALD, metal halides [151, 152], alkylamides [152] and alkyls [116] have been most commonly combined with NH_3 [116, 152] for film formation.

The next group is the phosphides, of which only AlP, GaP and InP have been presented. These processes mostly utilize toxic PH_3 as a precursor [153–155]. The metal precursors have also been fairly simple, including mainly alkyls [154, 156] and halides [153].

The only non-alkylsilyl-enabled ALD process for an antimonide, InSb, used the elements as precursors [157]. The ALE InSb served as an interface layer for further MBE growth. The best overall results were achieved when this interfacial layer was deposited at 300 °C with 85 atomic layers. This temperature is low for an ALE process [110], making the crystalline quality somewhat doubtful after only the ALE growth. The temperature was raised for the subsequent MBE, which should improve the crystallinity. The InSb growth was initially three dimensional, although the islands coalesced leading to two dimensional growth already after 40 cycles. The ALE InSb interfacial layer improved the crystallinity, optical and electrical properties of the 5 μm InSb film deposited by MBE [157].

As III-V semiconductors have industrially important properties, arsenides, in particular, have been the focus of intense study. In general, arsenides have been formed by ALE/ALD using arsine as the arsenic precursor. Compounds were generally used for group III precursors, as the elements have a low vapor pressure [110]. Thus the metal precursors have been fairly varied, including halides [158, 159], alkyls [160–162], amines [163] and cyclopentadienyls [164]. Other arsenic sources have been aminoarsine [164, 165] and tert-butylarsine [166, 167].

A good example is the quintessential III-V compound GaAs, which became the focus of intense study in the 1980s [160, 168] when the deposition method was still called ALE, atomic layer epitaxy. Though there were numerous studies on the subject [169], the epitaxial films were deposited with a limited number of precursor combinations, of which the combination of trimethyl gallium and arsine was the most popular. Hydrides in general have proven themselves as very good precursors, although in this case, precautions need to be taken. Arsine is very toxic and as a gas requires good safety measures.

Other alkyl gallium precursors [170, 171] were also used, along with gallium halides [158, 172, 173]. In addition, as mentioned earlier, alkyl compounds of arsine [174, 175] were also used as arsenic precursors. Practically all of these processes had growth rates that saturated to 1 ML/cycle, making the processes very stable.

The consistent problem with ALE GaAs processes was carbon contamination. Both trimethyl and triethyl gallium are thermally unstable and can crack before reaching the substrate or on the substrate [110]. Therefore, the gallium arsenide films were consistently p-type, if preventative measures were not taken to prevent this carbon contamination. Arsine doses needed to be sufficiently large and the gallium alkyl pulses short to achieve higher purity [111]

These days, most carrier gases used in ALD are inert. Curiously, in the GaAs studies, hydrogen was most often used as either the transport gas or even as a third precursor [176, 177]. Laser-assisted ALE was also used to ensure complete reactions on the surface. [178] Furthermore, the temperature range of these processes was limited to high temperatures, in the order of $300 - 500\ ^{\circ}\mathrm{C}$. This temperature could be too high for some applications and more sensitive substrates.

3.3 Alkylsilyl compounds as precursors

Alkylsilyl compounds are a recent addition to the ALD precursor toolbox [1]. They can be described with a general formula $(R_3Si)_xNm$, where R is an alkyl group and Nm is a chalcogen or pnictogen. The number x is determined by the non-metal as chalcogens require two and pnictogens three ligands. An example of a crystalline structure of an alkylsilyl tellurium compound, $(^{t}BuMe_2Si)_2Te$, can be found in Figure 3.3.

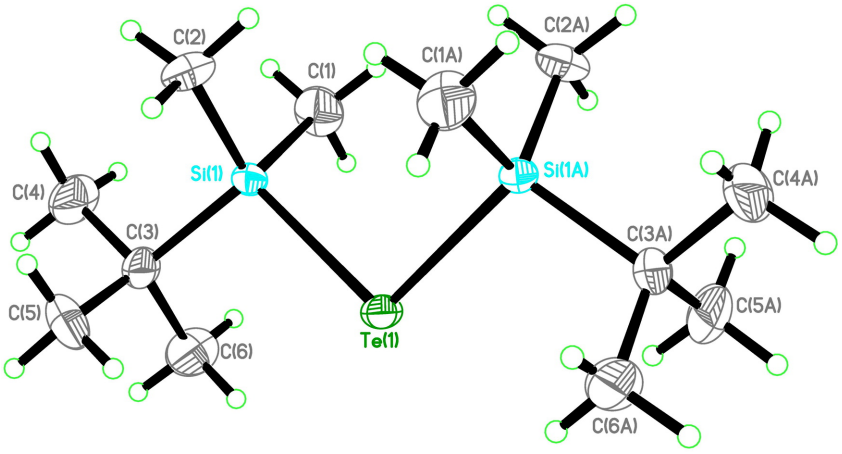

Figure 3.3: Molecular structure of $(^{t}BuMe_2Si)_2Te$. Reprinted with permission from [1]. Copyright (2009) American Chemical Society.

Alkylsilyl related chemistry is not new as such. For example, $(Me_3Si)_3As$ was combined with gallium and indium halides to form GaAs and InAs in the liquid phase already in 1989 [179]. The dehalosilylation reaction has also been utilized in the synthesis of other III-V materials [180], such as GaSb nanoparticles [181]. Even single-source precursors have been synthesized [182, 183].

The initial applicability of a precursor for ALD can be determined by thermo-gravimetric analysis (TGA). As the temperature of the sample is raised, the precursor weight loss should proceed in a single step. This would mean a clean evaporation and thus good applicability as a precursor. If the final residue is also close to 0, the thermal stability of the compound, another ALD requirement, is good. However, as the TGA method is based on the weight loss of the solid or liquid form, no further information about the gaseous product can be deduced [122]. TGA curves for several alkylsilyl chalcogenides and pnictides can be found in Figure 3.4.

All of the presented compounds show a single step evaporation, which indicates good volatility. Most of them also had very low residues, indicating that they do not decompose while evaporating. Some differences, however, could still be found. The compounds with methylsilyl ligands evaporated at lower temperatures than their counterparts with larger alkyl groups. The telluride compounds are a clear example of this behavior. $(Me_3Si)_2Te$ shows evaporation already below 50 °C, while $(^{t}BuMe_2Si)_2Te$ and $(Et_3Si)_2Te$ start to evaporate around 100 °C. There was also molecular weight dependency in the volatility, as group 15 alkylsilyls evaporated at higher temperatures than group 16 alkylsilyls. In addition, there were some residues for group 15, increasing from arsenic to antimony to bismuth, indicating some decomposition.

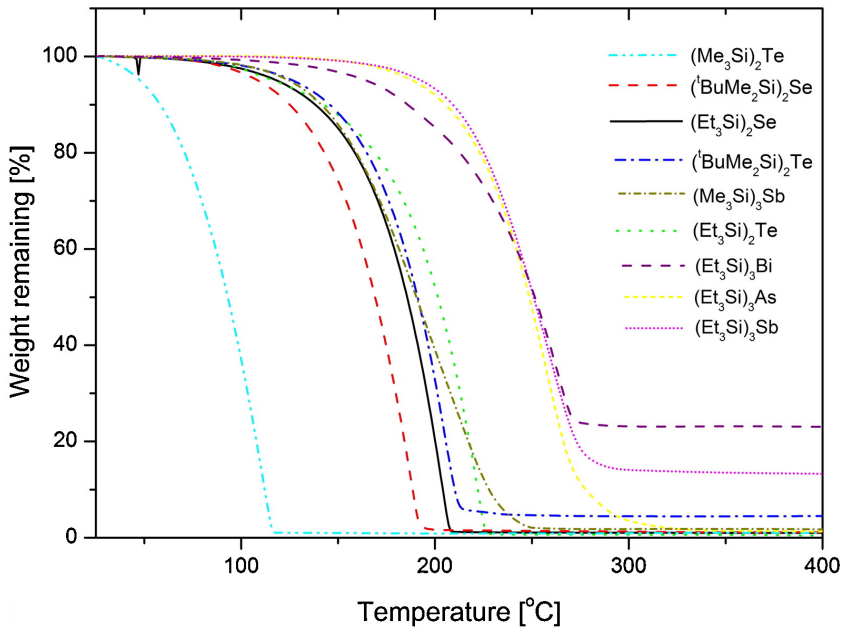

Figure 3.4: TGA curves for various alkylsilyl compounds of group 15 and 16 elements [184].

The use of alkylsilyl compounds with metal chlorides in ALD is based on very specific reactions, namely dehalosilylation reactions. The reactions can be understood in terms of the Lewis hard-soft acid-base (HSAB) theory, which states that hard acids and bases are small and only slightly polarizable species, while soft acids and bases are larger and more polarizable [185]. In the alkylsilyl compounds, silicon is a hard acid that is bonded to a large soft base such as selenium or tellurium. In the second precursor, the chloride is a fairly hard base, bonded to a possibly soft and large metal cation such as antimony(III). When the ligand exchange occurs, the results are more favorable hard-hard and soft-soft pairs of silicon-chloride and metal-chalcogen -pairs [122]. Examples of these dechlorosilylation reactions are presented in Equations (3.1)-(3.3).

$$2\,\mathrm{SbCl_3(g)} + 3\,(\mathrm{Et_3Si})_2\mathrm{Te(g)} \longrightarrow \mathrm{Sb_2Te_3(s)} + 6\,\mathrm{Et_3SiCl(g)} \tag{3.1}$$

$$\mathrm{GeCl_2 \cdot C_4H_8O_2(g)} + (\mathrm{Et_3Si})_2\mathrm{Te(g)} \longrightarrow \mathrm{GeTe(s)} + 2\,\mathrm{Et_3SiCl(g)} + \mathrm{C_4H_8O_2(g)} \tag{3.2}$$

$$\mathrm{SbCl_3(g)} + (\mathrm{Et_3Si})_3\mathrm{Sb(g)} \longrightarrow 2\,\mathrm{Sb(s)} + 3\,\mathrm{Et_3SiCl(g)} \tag{3.3}$$

Equation (3.1) is representative of all the dechlorosilylation reactions. The overall reactions are identical, whether the alkylsilyl compound is a chalcogenide or a pnictide. Consequently, making selenides or arsenides does not differ from depositing tellurides. Moreover, the oxidation state of the cation is not significant for the reaction. $GeTe_2$ can deposited as efficiently as the more common GeTe [186, 187].

The dehalosilylation reaction is not disturbed by an additional neutral ligand such as 1,4-dioxane in Equation (3.2). According to mechanistic studies, the dioxane ligand is completely released during the $GeCl_2 \cdot C_4H_8O_2$ pulse [188]. A special example of the utilization of the dechlorosilylation reaction is the formation of elemental antimony (Eq. (3.3)), which is enabled by the disproportionation reaction of antimony [I].

The similar reactions, and the self-limiting nature of ALD, give a good way to deposit ternary materials by combining binary processes. When Equations (3.1) and (3.2) are combined, the result is a GST process. When GeTe and Sb_2Te_3 are pulsed alternately, $Ge_2Sb_2Te_5$ can be formed [1]. When all three of the above ALD processes are combined in various deposition cycle ratios, the compositions can be controlled over a wide range.

All alkylsilyl compounds mentioned here are air and moisture sensitive, although somewhat less so when the alkylsilyl groups are large. This means that they need to be handled carefully while loading them into a reactor. Ethyl- and methylsilyl compounds are liquids and tert-butylsilyls are low-melting solids [122]. The former are thus good ALD precursors also for industrial applications since the surface area of a liquid does not change, keeping the precursor dose constant. The vapor pressure of the methyl silyl compounds is relatively high, making them easy to deliver in large doses but increasing the safety risk to some extent.

Chapter 4

Experimental

4.1 Atomic layer deposition of chalcogenide and pnictide thin films

All thin films in the studies included in this thesis were deposited in a hot-wall, flow-type F120 ALD reactor (ASM Microchemistry Oy, Helsinki, Finland). Nitrogen was used as the carrier and purge gas, with the operating pressure being below 10 mbar. The nitrogen was made on-site with a Nitrox UHPN 3000 generator (rated purity 99.9995 %)

The reactor design limits the size of the substrates, all of which were 5×5 cm^2. The most commonly used substrate materials were native SiO_2 -terminated silicon and soda-lime glass. Silicon substrates were used for most of the results that follow, while soda-lime glass was used for reflectivity and some of the resistivity measurements.

Each precursor was housed separately inside the reactor, evaporated from open glass vessels and heated individually to the required temperatures. $GeCl_2 \cdot C_4H_8O_2$ is a white needle-like solid, evaporated at 65 °C. $GaCl_3$, $SbCl_3$ and $BiCl_3$ are white powders, evaporated at room temperature, 30 and 140 °C. $GaCl_3$ has such a high volatility and reactivity with air that more careful handling is required than with the other chlorides as HCl is easily released. All alkylsilyl compounds used were liquids. $(Et_3Si)_2Se$, $(Et_3Si)_2Te$, $(Et_3Si)_3As$ and $(Et_3Si)_3Sb$ were evaporated at 35, 40, 80 and 85 °C, respectively. Extra precautions, such as a gas mask and gas detector were used when necessary, especially in the case of $(Et_3Si)_3As$. Precursor pulsing was performed with inert gas valving.

4.2 Chalcogenide and pnictide thin film characterization

Scanning electron microscope images were acquired using a Hitachi S-4800 field emission scanning electron microscope (FESEM). Film thicknesses and compositions were determined from energy dispersive X-ray (EDX) spectra, measured using an INCA Energy 350 EDX spectrometer connected to the S-4800. The measured k-ratios were transformed into thickness values by using a GMR electron probe thin film microanalysis program [189].

Light impurities were analyzed using time-of-flight elastic recoil detection analysis (TOF-ERDA), with a 5 MV tandem accelerator EGP-10-II, using 45 MeV ^{127}I or 48 MeV ^{79}Br as a primary beam. In another setup, also 8 MeV ^{35}Cl incident ions were used.

Films were also analyzed with Rutherford backscattering spectrometrry (RBS) using a 4.8 MeV He beam and a silicon detector located at 169 degrees.

Transmission electron microscopy (TEM) was performed with a FEI Tecnai F20 200 kV transmission electron microscope. Samples were prepared with a FEI Quanta 3D 200i DualBeam focused ion beam/scanning electron microscope (FIB/SEM).

When applicable, thicknesses were also determined by X-ray reflectivity (XRR) measurements with a Bruker D8 Advance X-ray diffractometer. Film crystallinity was analyzed with grazing incidence X-ray diffraction (GIXRD) and $\theta - 2\theta$ measurements using a PANalytical X'Pert Pro MPD X-ray diffractometer. For *in situ* high temperature XRD (HTXRD) measurements, an Anton-Paar HTK1200N oven was used.

Atomic force microscopy was performed with a Veeco Instruments Multimode V with a Nanoscope V controller. Samples were measured in tapping mode in air using phosphorus-doped silicon probes (RTESP, Veeco Instruments) or silicon probes (RFESP, Bruker).

Crystallization times of phase change materials were measured using a static laser tester. For crystallization studies, an amorphous sample was exposed to laser pulses of variable length and power. For recrystallization studies, the sample was first crystallized by annealing and then melt-quenched by laser pulses. Recrystallization was then attempted by applying pulses of variable power and time to the same location.

The electrical properties were measured with an Ecopia HMS-5000 Hall Effect Measurement system. Measurements were made in a 0.55 T magnetic field using the van der Pauw configuration in a temperature range from 80 to 350 K. Small indium droplets were used to contact the thin films. Routine resistivity measurements were made with a four point probe (CPS Probe Station, Cascade Microtech) connected to a Keithley 2400 source meter.

Resistivity as a function of temperature was measured from phase change materials using a custom-made set-up. Two large aluminum pads with a small and well defined gap were deposited prior to the measurements and were contacted by two contact pins. The resistance between the pins was measured during heating with a rate of 1 Ks^{-1}.

Thermoelectric measurements were performed on glass substrates heated from one end by a heat plate. Voltages were measured with a Keithley 2400 source meter and substrate temperatures with a simple K-type probe attached to a multimeter.

Surface analysis by low-energy ion-scattering (LEIS) was performed at Tascon GmbH, using an ION-TOF Qtac100 dedicated LEIS instrument. An overview of all elements heavier than B were achieved with 3 keV $^4He^+$ ions; 5 keV $^{20}Ne^+$ ions were used for a quantitative analysis of Bi and Te. The primary ion doses for the analyses were 1.4×10^{14} He ions/cm^2 and 3×10^{13} Ne ions/cm^2. Quantification was performed by means of statistical calibration. The samples were analysed 'as received' after shipping, and after *in situ* cleaning with O atoms for 10 minutes to remove hydrocarbon contamination. The statistical calibration was performed on the cleaned, and thereby well-defined samples.

Chapter 5

Results and discussion

Alkylsilyl chalcogenides and pnictides have already enabled a large number of ALD processes through the dehalosilylation reactions. When combined with chloride precursors, many previously unseen materials, such as GeTe, Sb and Bi_2Se_3, can now be made by ALD. In addition, some new routes are provided for materials like ZnTe and GaAs that had also been deposited by ALD earlier. All of the ALD processes demonstrated so far with alkylsilyl non-metal precursors are presented in Figure 5.1. In this chapter, aspects of some of these ALD processes, mainly those of Sb [I], GeTe [II], Bi_2Te_3 [III], Bi_2Se_3 [IV] and GaAs [V] are studied more closely.

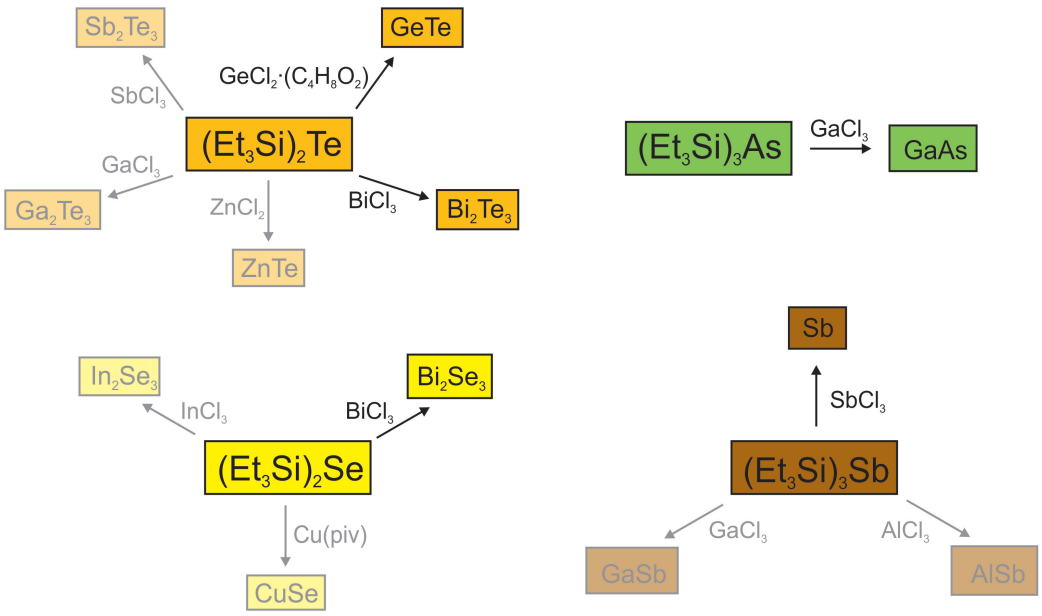

Figure 5.1: ALD processes enabled by non-metal alkylsilyl precursors.

5.1 Properties of chalcogenide and pnictide ALD processes

Although a large number of ALD processes with different precursors are covered in this thesis, they are remarkably similar in many respects. The underlying reason must be the chemistry that these processes share. The dehalosilylation reactions presented in Section 3.3 ensure that the end results must be similar. This section delves closely into the characteristics of the ALD processes and their similarities.

5.1.1 Growth rate saturation

Growth rate saturation is the key property in defining a process to be true ALD. The growth rate of thin films should saturate after a sufficiently large precursor dose is received, which ensures reactions with all available surface groups. Figures 5.2 and 5.3 show that this condition is fulfilled in all processes that use alkylsilyl precursors.

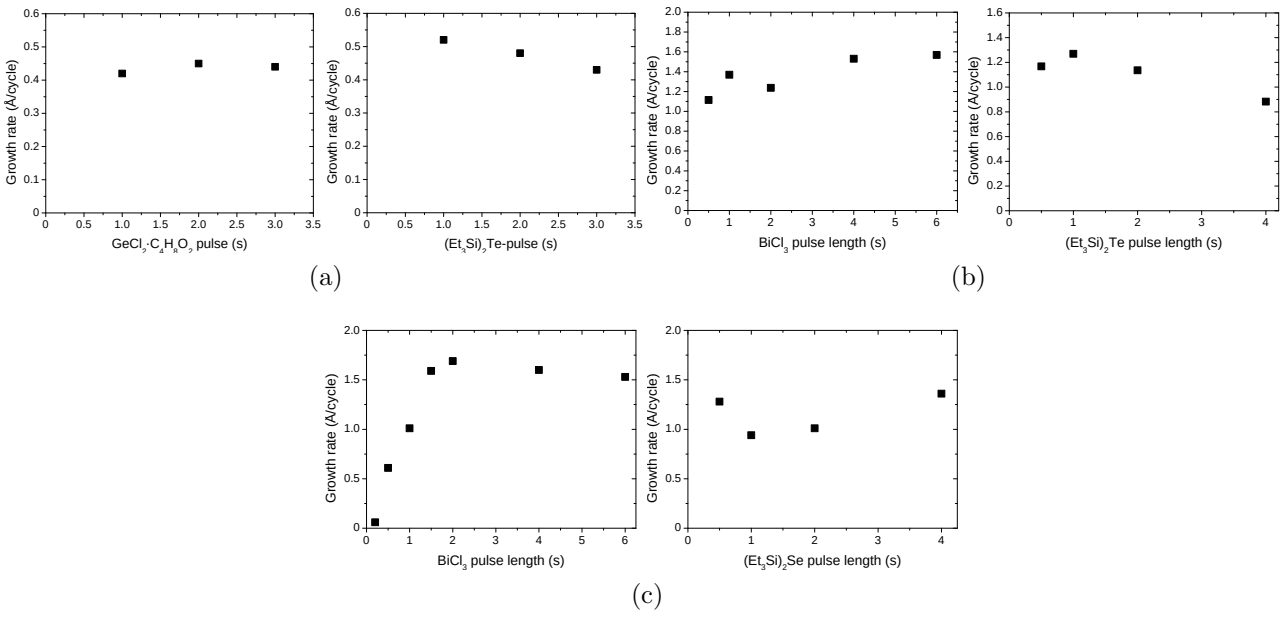

Figure 5.2: Effect of precursor pulse lengths on the growth rate of GeTe [II] (a), Bi_2Te_3 [III] (b) and Bi_2Se_3 [IV] (c) thin films.

Both telluride processes, GeTe and Bi_2Te_3, show very similar characteristics with respect to $(Et_3Si)_2Te$. There is saturation from early on with 1 s pulses. After that, there might even be a decline in growth rates when precursor pulse lengths are increased. The reasons for this might be similar to those for the purge effects, discussed in Section 5.1.2.

The only selenide process Bi_2Se_3, differs somewhat from the telluride processes. There appears to be a slight increase in the growth rate after the stable growth region is achieved. Either the $(Et_3Si)_2Se$ is slower to adsorb and react on the surface than $(Et_3Si)_2Te$, or the slight drift might just be due to a measurement uncertainty from the EDX or due to minor differences in deposition temperature. There was a strong temperature dependence of the growth rate, discussed in detail in Section 5.1.3.

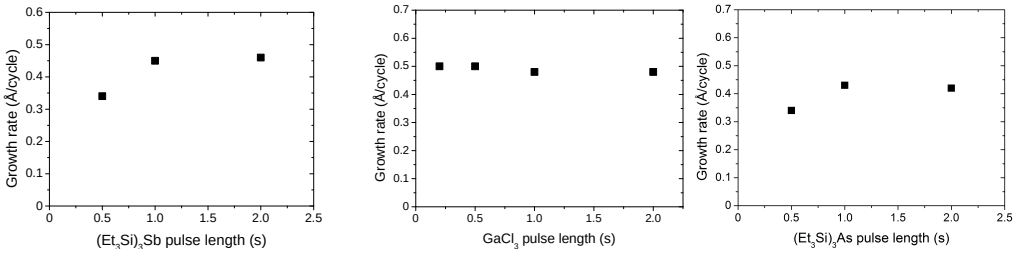

(a) (b)

Figure 5.3: Effect of precursor pulse lengths on the growth rate of Sb [I] (a) and GaAs [V] (b) thin films.

It appears that the pnictide processes GaAs and Sb behave similarly to each other. Saturation with $(Et_3Si)_3As$ and $(Et_3Si)_3Sb$ was achieved with 1 s pulses, after which the changes in growth rates were minor.

As for the counterparts of the alkylsilyls, the metal or semimetal precursors, their saturation behavior was very straightforward. Most saturated almost immediately, only $BiCl_3$ needed longer pulses to reach the growth rate saturation. The films deposited with shorter pulses showed no differences in properties when compared to the films deposited with pulses further in the saturation region.

Overall, proper ALD-like growth rate saturation behavior can be found in all of the alkylsilyl-enabled processes. This saturation leads to repeatability and process stability, which enables parameter tweaking for the desired reactor types and applications.

5.1.2 Purge effects

In general, purges should not have an effect on ALD processes, as long as they are sufficient in removing all the excess precursors and by-products. Therefore, it was somewhat surprising that the lengths of purges affected the growth of Bi_2Te_3 and Bi_2Se_3 so drastically. An example with Bi_2Se_3 is given in Figure 5.4.

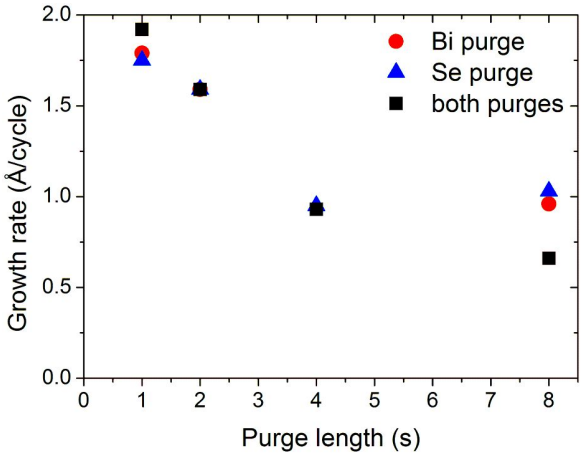

Figure 5.4: Effect of purge lengths on the growth rate of Bi_2Se_3 thin films [IV].

When only the purge after one precursor was increased from 1 to 8 s, the growth rate halved. The overall decrease in growth rate was up to two thirds, when both purges were increased at the same time. The reasons for this can be multitudinous. The adsorption might not be complete immediately, and there could be some physisorption involved. This would mean that the unreacted groups have more time to desorb from the surface, pushed along with the purge gas flow.

Similar behavior has been seen in a GST process using alkoxides and alkylsilyl telluride where precursor adsorption and desorption were balanced, allowing for ALD-like saturation behavior in combination with the significant decrease in growth rate with respect to increasing purge lengths [186]. Reaction mechanism studies on the Sb_2Te_3 process [188] have shown, however, that a ligand exchange reaction occurs during both pulses. After such a reaction, the desorption should be more difficult than in the case of chemisorption alone. Partial desorption is still possible, possibly through ligand rearrangement.

5.1.3 Temperature dependence

The most striking property of the alkylsilyl ALD processes is their strong temperature dependence. As discussed in Section 3.1, many ALD processes have growth rates that stay nearly constant within a range of temperatures. This was definitely not the case for the chalcogenide processes shown in Figure 5.5a.

All the processes showed a similar trend of a pronounced decrease in the growth rate with increasing deposition temperatures. This was not connected to the absolute deposition temperatures, since Bi_2Te_3 and Bi_2Se_3 could be deposited at much higher temperatures than GeTe or Sb_2Te_3. In fact, Bi_2Te_3 and Bi_2Se_3 deposition occurs at temperatures, where GeTe or Sb_2Te_3 no longer grow at all. In addition, ZnTe and ZnSe have been deposited at much higher temperatures (400 °C) than Bi_2Te_3 and Bi_2Se_3. Nevertheless, all of the chalcogenide processes follow the trend of decreasing growth rates within their own temperature range.

The pnictide processes (Figure 5.5b) mostly behave in the same way as the chalcogenides. The only difference is that both Sb and GaAs processes show a plateau of sorts in the middle of their deposition temperature range. The usual explanation for this overall growth rate decrease would be precursor desorption or a decrease in the density of the reactive sites. This type of behavior is not restricted to alkylsilyl-enabled ALD processes - a similar temperature dependence was also seen in ALD of AlF_3 [190], for example.

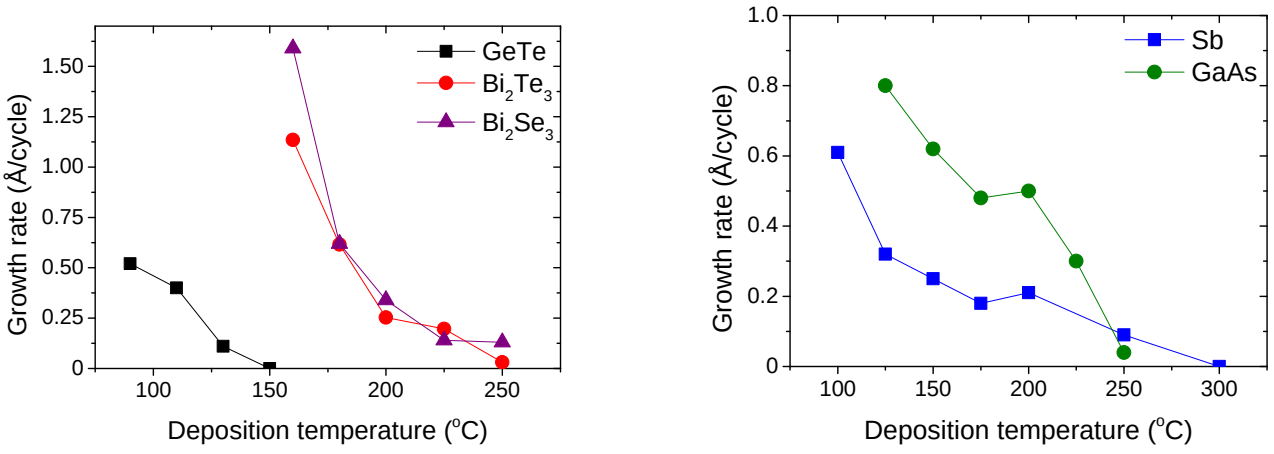

(a) (b)

Figure 5.5: Effect of deposition temperature on the growth rate of chalcogenide (a) and pnictide (b) thin films.

Similar temperature effects have been seen with MBE [35] and sputtering [191] of tellurides. A suggested reason for this kind of behavior has been the high vapor pressure of tellurium, which as a continuous flux can even etch a whole film away [35, 36].

5.1.4 Film growth

As can be expected of proper ALD processes, all alkylsilyl processes enable efficient film thickness control. Regardless of the temperature dependence or purge related behavior, film thickness was always determined by the number of deposition cycles. There appeared to have been no incubation periods in any of the processes, as the relation between the film thickness and the number of deposition cycles was linear from the very beginning.

Nevertheless, this did not mean that growth progressed in the quintessential layer-by-layer mode. It could have been the case with the processes that produced amorphous films, but LEIS has indicated that growth may very well follow the island-growth mode in the early stages of processes producing crystalline films [III].

The initial stages of Bi_2Te_3 film growth were followed with LEIS, the results of which can be seen in Figure 5.6. In Figure 5.6a, the silicon signal slowly disappeared as the bismuth and tellurium signals increased, indicating that the film was closing over the substrate surface. Full closure occurred after about 70-90 deposition cycles, which would mean a film thickness of about 10 nm according to EDX. LEIS revealed another interesting aspect of the early Bi_2Te_3 film growth, namely the changing composition of the outermost layer of the growing film. In Figure 5.6b, it can be seen that mostly bismuth is deposited during the first few cycles, even though $(Et_3Si)_2Te$ was pulsed last in the cycle. Close to stoichiometric, and stabilized, ratios of Bi and Te could be found on the surface after eight deposition cycles [III].

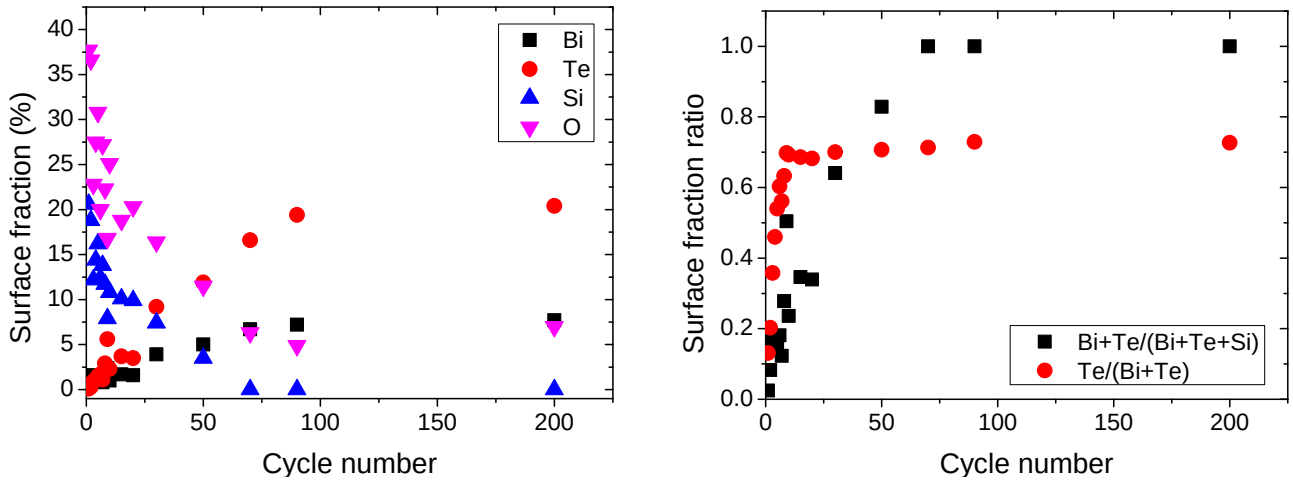

(a) (b)

Figure 5.6: Surface fraction of the elements (a) and their ratios with respect to the number of deposition cycles (b), measured with LEIS [III].

5.1.5 Conformality

The self-limiting saturative growth that defines ALD enables conformal deposition onto high aspect ratio substrates. As the precursors are transported to the substrate in the gas phase, they can react with all available surfaces, assuming the precursor molecule is small enough to physically fit into the possible crevices. A good example can be seen in Figure 5.7.

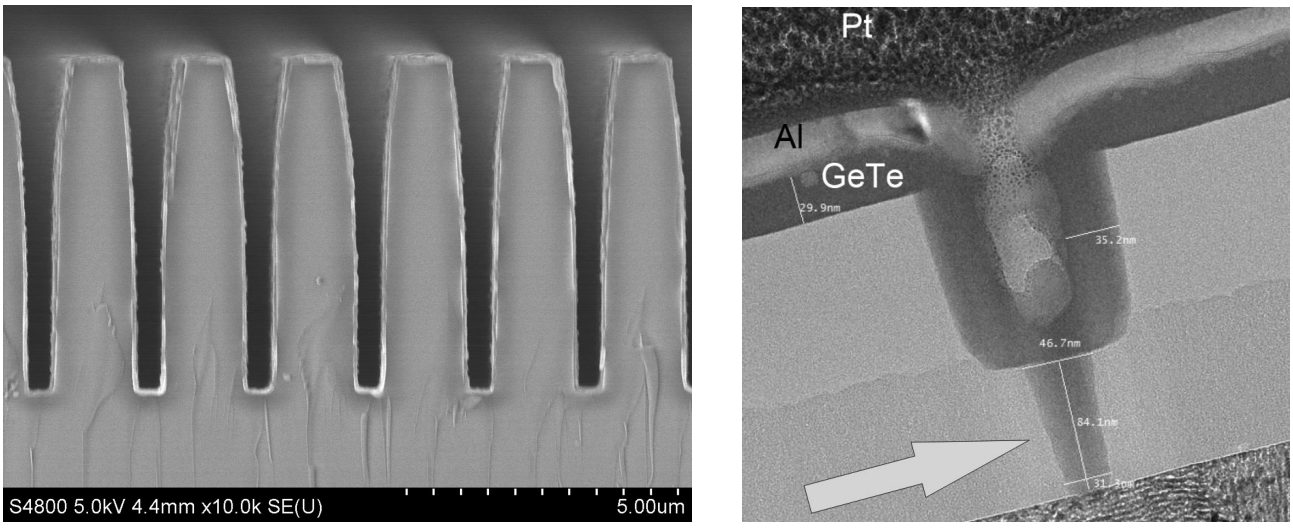

(a) (b)

Figure 5.7: FESEM image of Sb (a) and a TEM image of GeTe [II] (b) thin films deposited onto demanding three-dimensional substrates.

In Figure 5.7a, the Sb film follows the surface of the trench structure closely. The film thickness appears equal on both the top surface and at the bottom of the trench, as well as on the side walls. Similar behavior is demonstrated by the GeTe film in Figure 5.7b. The GeTe film was deposited into a 31 × 84 nm via at the bottom of the trench. The via is completely filled, the film follows the substrate shape with little thickness variation, without a visible seam. These two processes are a good example of ALD conformality, as the Sb produces crystalline films and the GeTe process amorphous films. This crystallinity difference has no meaning for the inherent properties of ALD, and good conformality is the end result. Conformality is especially important for applications like phase change memories, where the memory element is located in a tight space like in Figure 2.2c. Voids or unevenness in the film can cause device malfunction. For complete via filling, an amorphous structure is more suitable because a polycrystalline film will produce a grain boundary in the middle of the via.

5.2 Properties of ALD chalcogenide and pnictide thin films

In addition to being notable additions to the materials selections of ALD processes, the chalcogenide and pnictide films should also be of good quality, and have the right properties to be industrially applicable. The ALD chalcogenide and pnictide thin films should present the properties needed for their most typical and intended applications. The following sections present studies on the properties of these thin films.

5.2.1 Composition

The chemistry of the dehalosilylation reaction has proven to be highly efficient in producing stoichiometric films in most deposition conditions. The correct composition is one of the most important properties a thin film must have. The chemistry should generally lead to stoichiometric compound formation and not just alloying, which maybe in some cases the desired result. These compositions should also be stable, and not affected by minor parameter changes.

The versatility of ALD can be seen when different binary processes are mixed to form ternaries. This was definitely the case for phase change materials, where the binary processes were highly compatible. By combining GeTe, Sb_2Te_3, GeSb and Sb processes in the same deposition, numerous compositions within the phase diagram in Figure 5.8 were achieved.

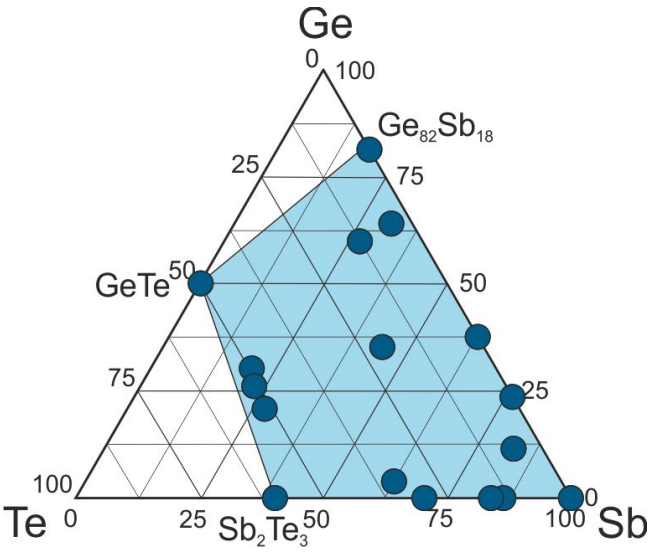

Figure 5.8: Compositions of ALD phase change materials. Filled circles represent examples of measured EDX compositions of thin films. Reprinted from [122] with permission from Elsevier, Copyright (2013).

In the instance of thermoelectric materials Bi_2Te_3 and Bi_2Se_3, the deposition processes were also in this aspect practically identical. Both processes produced n-type chalcogen-rich films in all deposition conditions. The compositional stability is excellent for repeatability, although thermoelectric materials are usually tailored alloys, where both p- and n-types are needed.

In the Sb process, the disproportionation reaction between the two Sb-containing precursors can only lead to elemental Sb, which was also the case. Even such a reaction still leaves a great deal to be studied composition-wise. For example, impurities are very important factors in determining other film properties.

The only greater variations in compositions were seen in the GaAs process. According to EDX, stoichiometric films in terms of the Ga/As ratio were produced only at the ALD window temperature of 200 °C. This was also verified with RBS, meaning that the chemistry was not as stable as it was with all the other alkylsilyl processes, where the temperature did not affect the composition.

For the most part, alkylsilyl-enabled ALD processes produced very pure films. This is especially noteworthy when the deposition temperatures are considered. They vary between 80 and 160 °C, and are very low for typical ALD processes. In general, higher deposition temperatures lead to less impurities in the films. As shown for the Sb process in Figure 5.9, in the films discussed in this chapter, only a few atomic percent or fractions thereof of the most typical impurity elements, such as carbon, nitrogen, hydrogen, oxygen and chlorine, were found. In addition,

most of the oxygen was found on the surface of the films - the impurity contents within the films were even lower.

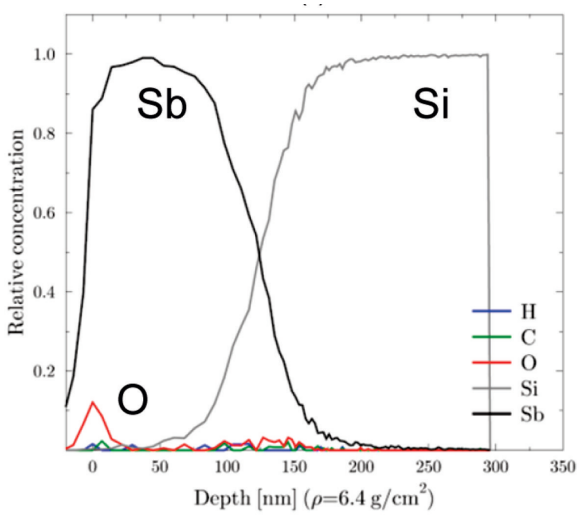

Figure 5.9: TOF-ERDA depth profile of an Sb thin film [I].

Gallium arsenide was the exception here as well. At low temperatures and long $GaCl_3$ pulses, the chlorine content was much higher, even about 20 at.% according to EDX. TOF-ERDA measurements from a film deposited at 200 °C indicated that most impurities were at the level of a single atomic per cent or less. Only the amount of oxygen was higher, and the exact location of the oxygen could not be determined. The most probable location is on the surface of the film, such as in Figure 5.9. Some of the impurities were most likely due to some incomplete reactions of $GaCl_3$. Overall, it seems that the GaAs process is the most unstable of the alkylsilyl-enabled ones.

5.2.2 Crystallinity and morphology

Crystallinity and morphology are very important thin film properties. Many applications require the film to be either amorphous or crystalline, and exist in the correct crystalline phase if there are many. It cannot be known beforehand whether a particular ALD process produces amorphous or crystalline films; and if crystalline, in what phase. The phase is influenced by deposition parameters, which need to be optimized. Undesirable phases are one reason to search for new precursors and chemistries. The ALD processes discussed in this thesis had crystallinity and morphology that were very much process dependent, and to some extent temperature dependent.

The only amorphous films were produced by the GeTe and GaAs processes. Also, most ternary phase change materials, with a sufficiently low content of either Sb or Sb_2Te_3, were amorphous as-deposited at the lowest deposition temperatures. This is good since amorphous materials are preferred in phase change applications due to smoother film surfaces.

For example, GeTe thin films could be crystallized only by annealing and not during the deposition. An example HTXRD is provided in Figure 5.10. The film stayed amorphous past the possible deposition temperature range and crystallized only at 165 °C. The initial crystallization formed a rhombohedral phase, which then transformed to the high-temperature cubic phase at 385 °C. All the peaks show a slow drift towards smaller 2θ values, more than only a thermal expansion would cause. In addition, the two peaks at about 43° combine into a single peak with the cubic transformation. The high-temperature cubic phase transformed back into the rhombohedral phase when cooled, and the double peaks could again be resolved [II]. This crystallization and diffraction behavior of ALD GeTe is very similar compared to literature values for sputtered GeTe [192].

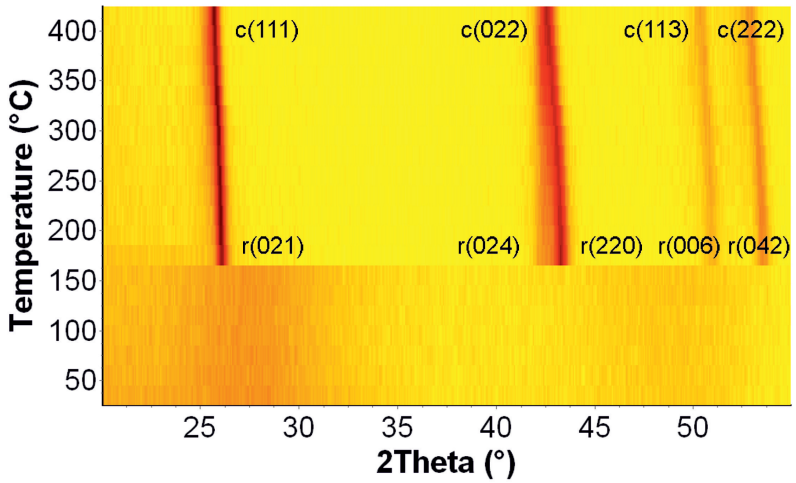

Figure 5.10: HTXRD of a GeTe thin film deposited at 90 °C [II].

The rhombohedral phase was the common denominator for Bi_2Te_3 and Bi_2Se_3. They both belong to the same space group, and thus have almost identical diffraction patterns. The slight differences in the diffraction patterns arise from the differences in the lattice parameters caused by the telluride ion being bigger than the selenide ion. The $\theta - 2\theta$ diffractograms of Bi_2Te_3 and Bi_2Se_3 were indeed very similar, as can be seen from Figure 5.11a. Both clearly show diffraction peaks arising from the same crystal planes, namely the (003) and its multiples. This is an indication of preferred orientation of growth in the (001), or the c-axis, direction.

The similarities were also seen in TEM, where the initial stages of growth for both Bi_2Te_3 and Bi_2Se_3 included oriented small grains. The TEM images in Figure 5.11b demonstrate the clear crystalline structure of the grains. The distance between the fringes in both images, about 1 nm, corresponded to the distance between the (003) planes in the crystal structure, which is the physical length of one quintuple layer, (Te/Se)-Bi-(Te/Se)-Bi-(Te/Se), of the material. The preferred orientation seen in XRD is thus confirmed by TEM. The growth of Bi_2Te_3 and Bi_2Se_3 proceeds mainly in the (001) direction.

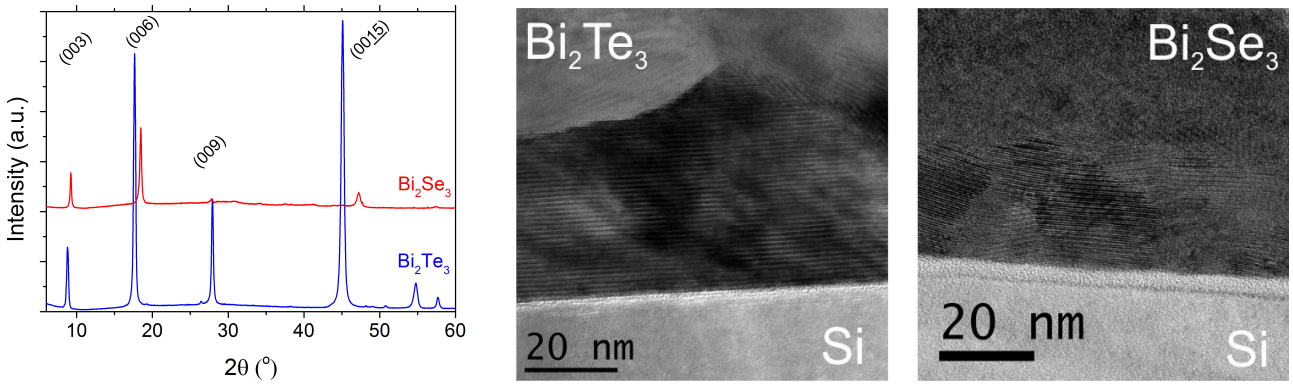

(a) (b)

Figure 5.11: XRD (a) and TEM (b) of Bi_2Te_3 and Bi_2Se_3 thin films deposited at 160 °C [III, IV].

The surface morphologies have been found to be a direct consequence of the crystalline structure of the growing films. Amorphous substances are naturally featureless on the surface, while in crystalline materials the differences in the original crystalline orientation and the growth rates of the different crystalline facets will cause roughness on the surface [193–195]. Examples are presented in Figure 5.12. There is little to be seen in the image of GeTe (Fig. 5.12a) as it was amorphous. Sb_2Te_3 (Fig. 5.12b) and Bi_2Te_3 (Fig. 5.12c), on the other hand, show practically identical surface structures of flakes. This stems from the crystalline structures, which are both rhombohedral and belong to the space group 166. This type of flaky morphology exists at the very surface of the films, while the parts deeper in the film show a dense structure and firm attachment to the substrate, as seen in the TEM images above. The flaky surface structure is therefore likely to be caused by the cohesive failure within the crystallites of the film as it grows thicker.

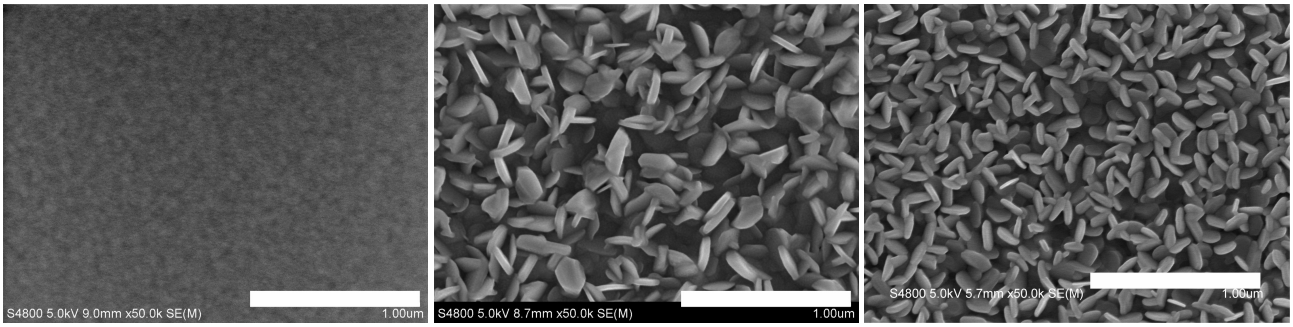

(a) (b) (c)

Figure 5.12: FESEM images of GeTe [II] (a), Sb_2Te_3 (b) and Bi_2Te_3 [III] (c) thin films. The scale bar in all images is 1 μm.

5.2.3 Phase change properties

Phase change memories rely on the phase change between the amorphous and crystalline phases. This change needs to be easy and repeatable. There also needs to be a clear difference in the optical and electrical properties between the phases. All of these requirements were fulfilled by ALD GeTe, and earlier also for ALD GST [196].

The optical changes are demonstrated in Figure 5.13, where a laser has been used to crystallize the amorphous as-deposited thin film (Fig. 5.13a), or to first melt-quench an annealed film and then recrystallize it (Fig. 5.13b). The results from these two images are in line with the literature, as recrystallization occurs much faster than the initial crystallization. This has been explained with small crystallites being left behind after melt-quenching [16]. In this case, the crystallization took place in 300 ns, which is a comparable value to those measured from sputtered films. The recrystallization occurred in only 50 ns, which is faster than that in sputtered films [II].

The electrical resistivity was also compared to the sputtered films. The behavior was again comparable, as can be seen from Figure 5.14. The only difference is the slightly higher crystallization temperature of the ALD GeTe, 185 °C. The difference in resistivity between amorphous and crystalline phases is more than enough for readout purposes or multilevel storage, six orders of magnitude [II].

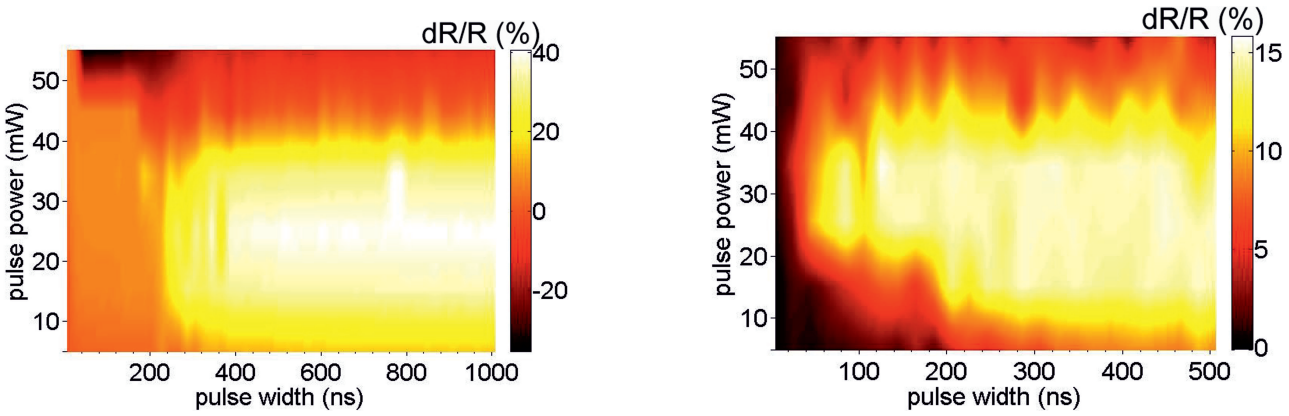

(a) (b)

Figure 5.13: Laser crystallization (a) and recrystallization of melt-quenched (b) GeTe [II].

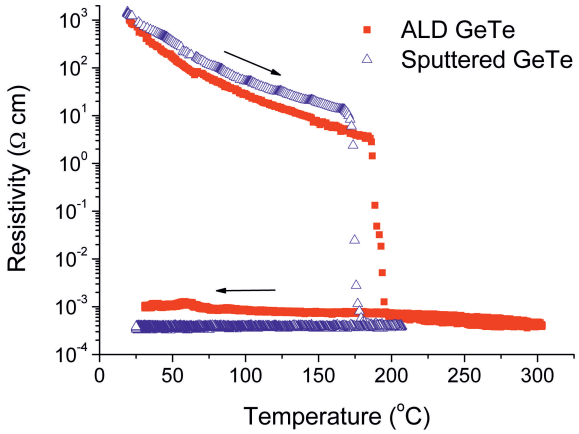

Figure 5.14: Resistivity of ALD (squares) and sputtered (triangles) GeTe [II].

It can be concluded that thin films made by ALD work at least just as well as the customary sputtered films. This has been shown here for GeTe, and previously also for GST [196].

5.2.4 Thermoelectric properties

The properties used for determining the thermoelectric applicability of a material are all found in the figure of merit ZT (Eq. 2.1). Electrical measurements bring out the differences between Bi_2Te_3 and Bi_2Se_3, as can be seen from Figure 5.15. As Bi_2Te_3 has much better conductivity than Bi_2Se_3, it is also fairly safe to assume that from these two ALD materials, Bi_2Te_3 would perform better as a thermoelectric material. Additionally, Bi_2Se_3 is most commonly alloyed in general and not so much used on its own as a thermoelectric.

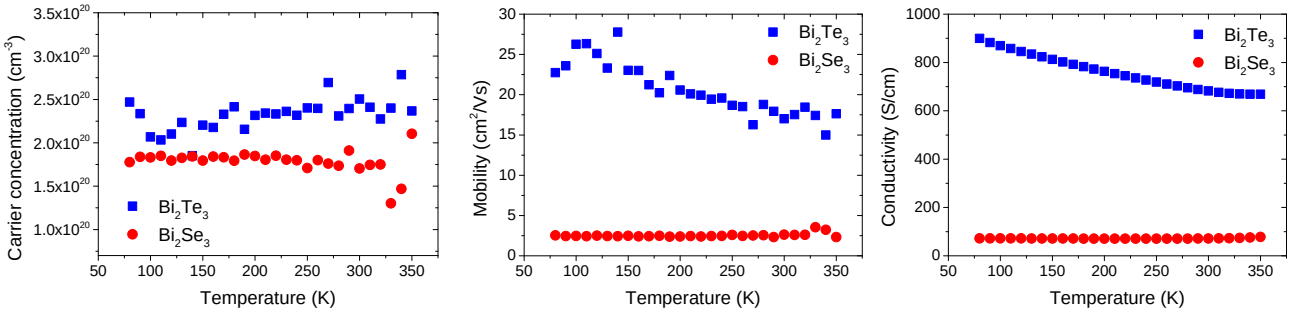

Figure 5.15: Temperature dependence of carrier concentration (a), mobility (b) and conductivity (c) of Bi_2Te_3 (squares) and Bi_2Se_3 (circles) thin films deposited at 160 °C [III].

The thermoelectric performance was studied with the setup from Figure 5.16. The results demonstrate clear thermoelectric behavior for both Bi_2Te_3 and Bi_2Se_3. Surprisingly, they behaved almost identically. Both measurements lead to slopes of $-180\ \mu V\ K^{-1}$, which agree very well with the literature values for n-type Bi_2Te_3 [49] and Bi_2Se_3 [77, 197–199].

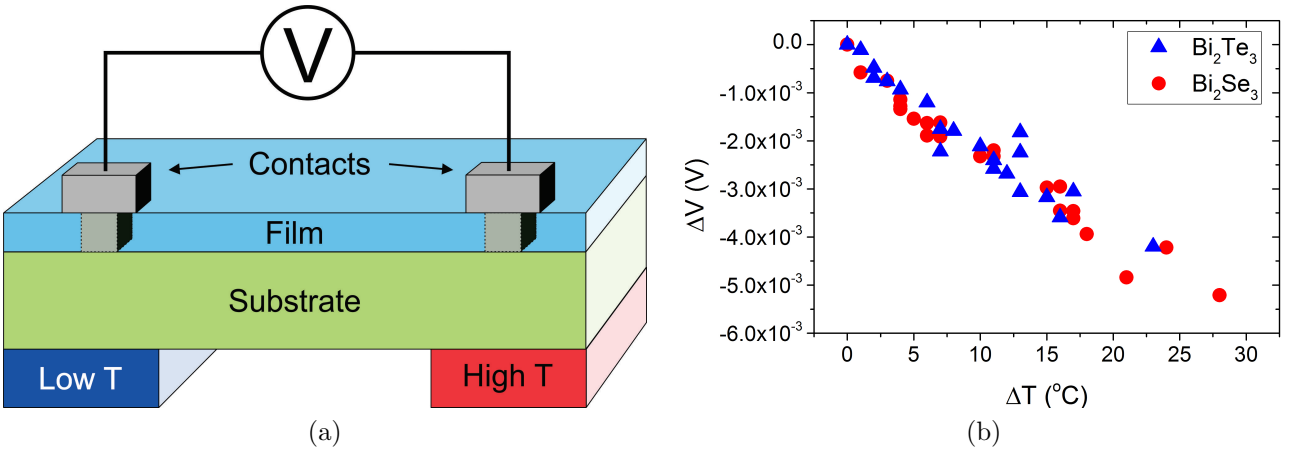

Figure 5.16: Thermoelectric measurement setup (a) and the thermoelectric response (b) of Bi_2Te_3 (triangles) and Bi_2Se_3 (circles) thin films deposited at 160 °C [IV].

Although ALD thin films have not been used in thermoelectric devices, the previous results prove that this could be possible. When the substantial thremoelectric response is combined with the good quality of the films and deposition processes themselves, ALD should be considered as a method to deposit thermoelectric materials for applications.

Chapter 6

Conclusions and outlook

The importance of materials and device engineering becomes increasingly evident as time goes by. The progress in the microelectronics industry, fueled by Moore's law, leads to smaller and smaller devices. The laws of physics will put an end to the shrinkage at some point. Eventually, new materials are needed and device structures become increasingly complicated and three-dimensional. It is this complexity that gives more opportunities for ALD to be used. In the end, some thin film structures can only be made with ALD due to the conformality of the method. This has led to a great increase in ALD research as can be seen from the increasing number of scientific papers published in the field. As a result, there is also a need for more application driven research. Applications need materials with specific compositions and properties.

Overall, the alkylsilyl compounds have proven to be excellent ALD precursors. They evaporate cleanly and have shown good temperature stability. With the deceptively simple dehalosilylation reaction, good quality thin films have been made. The processes themselves have presented all the necessary requirements of ALD. Growth rates saturate with respect to precursor pulse lengths; film thicknesses are easily controlled by the number of deposition cycles; and the films are conformally deposited on complex substrate surfaces.

Moreover, the ALD thin films themselves present excellent properties. Generally, films have been stoichiometric, with low impurity contents. Desired crystalline phases were observed, and even oriented growth was detected. In addition, the phase change and thermoelectric properties of the appropriate materials have been proven, which is essential for using ALD in those applications.

Further research ventures in to this area should delve into the reasons behind the untypical purge-related behavior seen with Bi_2Te_3 and Bi_2Se_3. The cause behind this behavior should be determined and whether it is more common or only limited to these particular processes.

One interesting avenue to follow would be making thermoelectric devices from ALD thin films. Since most devices are macroscopic in size, and the thermoelectric material made to bulk form, it presents an obvious challenge. Two questions to be addressed are: How thin can the devices be made? What kinds of structural changes in the device would be needed with a vapor deposition method?

In the phase change materials, there is still much of the Ge-Sb-Te phase diagram to be explored. Even though ALD of many compositions has been proven, only a few have been tested for repeatable phase change. In addition, as doping has always been an important part of phase change material tuning, other elements, such as gallium, could be introduced to the processes. This should not lead to any major compatibility issues, providing the dehalosilylation reaction is not disturbed.

There are still a number of chalcogenide and pnictide processes that have only been demonstrated to work. Further studies could be made on indium chalcogenides and aluminum pnictides, for example. It is evident that the dehalosilylation reaction will work for more precursor combinations than presented in this thesis.

The next possible materials to be explored with this alkylsilyl chemistry are the transition metal dichalcogenides (TMDC). They have become the "hot topic" in the research community due to their possibilities in the 2D scale. In general, 2D TMDCs have band gaps, which makes them usable in electronic applications where graphene cannot be used.

The processes demonstrated here cover a variety of technologically important materials. With the growing ALD market, it will be interesting to see whether some of these processes make it into production and onwards to the consumers. Nevertheless, there will definitely be a need for more ALD research, also with alkylsilyl non-metal precursors.

References

1. Pore, V., Hatanpää, T., Ritala, M., and Leskelä, M. *J. Am. Chem. Soc.* **131**(10), 3478–3480 (2009).

2. Ovshinsky, S. R. *Phys. Rev. Lett.* **21**(20), 1450–1453 (1968).

3. Wuttig, M. *Nat. Mater.* **4**(4), 265–266 (2005).

4. Wuttig, M. and Yamada, N. *Nat. Mater.* **6**(11), 824–832 (2007).

5. Elliott, S. R. In *Phase Change Materials: Science and Applications,* Raoux, S. and Wuttig, M., editors, 63–80. Springer Science & Business Media (2009).

6. Yamada, N., Ohno, E., Nishiuchi, K., Akahira, N., and Takao, M. *J. Appl. Phys.* **69**(5), 2849–2856 (1991).

7. Nirschl, T., Philipp, J., Happ, T., Burr, G., Rajendran, B., Lee, M., Schrott, A., Yang, M., Breitwisch, M., Chen, C., Joseph, E., Lamorey, M., Cheek, R., Chen, S.-H., Zaidi, S., Raoux, S., Chen, Y., Zhu, Y., Bergmann, R., Lung, H., and Lam, C. In *Int. Electron Devices Meet.*, 461–464, (2007).

8. Cassinerio, M., Ciocchini, N., and Ielmini, D. *Adv. Mater.* **25**(41), 5975–5980 (2013).

9. Lacaita, A. L. and Redaelli, A. *Microelectron. Eng.* **109**, 351–356 (2013).

10. Elliott, S. R. *Int. J. Appl. Glass Sci.* **6**(1), 15–18 (2015).

11. Raoux, S. and Wuttig, M., editors. *Phase Change Materials: Science and Applications.* Springer Science & Business Media, (2009).

12. Veiko, V., Ageev, E., Kolobov, A. V., and Tominaga, J. *J. Optoelectron. Adv. M.* **15**(5–6), 371–394 (2013).

13. Adler, D., Henisch, H. K., and Mott, S. N. *Rev. Mod. Phys.* **50**(2), 209–220 (1978).

14. Raoux, S., Shelby, R., Muñoz, B., Hitzbleck, M., Krebs, D., Salinga, M., Woda, M., Austgen, M., Chung, K., and Wuttig, M. In *E*PCOS 2008.*

15. Raoux, S., Welnic, W., and Ielmini, D. *Chem. Rev.* **110**(1), 240–267 (2010).

16. Cheng, H.-Y., Raoux, S., and Chen, Y.-C. *J. Appl. Phys.* **107**(7), 074308 (2010).

17. Loke, D., Lee, T. H., Wang, W. J., Shi, L. P., Zhao, R., Yeo, Y. C., Chong, T. C., and Elliott, S. R. *Science* **336**(6088), 1566–1569 (2012).

18. Terao, M., Morikawa, T., and Ohta, T. *Jpn. J. Appl. Phys.* **48**(8), 080001 (2009).

19. Bruns, G., Merkelbach, P., Schlockermann, C., Salinga, M., Wuttig, M., Happ, T. D., Philipp, J. B., and Kund, M. *Appl. Phys. Lett.* **95**(4), 043108 (2009).

20. Shi, L. In *Phase Change Materials: Science and Applications,* Raoux, S. and Wuttig, M., editors, 253–284. Springer Science & Business Media (2009).

21. Lee, S.-H., Hwang, Y., Lee, S., Ryoo, K., Ahn, S., Koo, H., Jeong, C., Kim, K., Koh, G., Jeong, G., Jeong, H., and Kim, K. In *Symp. on VLSI Tech.*, 20–21, (2004).

22. Pellizzer, F., Pirovano, A., Ottogalli, F., Magistretti, M., Scaravaggi, M., Zuliani, P., Tosi, M., Benvenuti, A., Besana, P., Cadeo, S., Marangon, T., Morandi, R., Piva, R., Spandre, A., Zonca, R., Modelli, A., Varesi, E., Lowrey, T., Lacaita, A., Casagrande, G., Cappelletti, P., and Bez, R. In *Symp. on VLSI Tech.*, 18–19, (2004).

23. Breitwisch, M., Nirschl, T., Chen, C., Zhu, Y., Lee, M., Lamorey, M., Burr, G., Joseph, E., Schrott, A., Philipp, J., Cheek, R., Happ, T., Chen, S.-H., Zaidi, S., Flaitz, P., Bruley, J., Dasaka, R., Rajendran, B., Rossnage, S., Yang, M., Chen, Y., Bergmann, R., Lung, H., and Lam, C. In *Symp. on VLSI Tech.*, 100–101, (2007).

24. Lacaita, A. *Solid-State Electron.* **50**(1), 24–31 (2006).

25. Kolobov, A. V., Fons, P., Frenkel, A. I., Ankudinov, A. L., Tominaga, J., and Uruga, T. *Nat. Mater.* **3**(10), 703–708 (2004).

26. Wuttig, M. and Raoux, S. *Z. Anorg. Allg. Chem.* **638**(15), 2455–2465 (2012).

27. Shportko, K., Kremers, S., Woda, M., Lencer, D., Robertson, J., and Wuttig, M. *Nat. Mater.* **7**(8), 653–658 (2008).

28. Lencer, D., Salinga, M., Grabowski, B., Hickel, T., Neugebauer, J., and Wuttig, M. *Nat. Mater.* **7**(12), 972–977 (2008).

29. Baldwin, R. A., Foos, E. E., and Wells, R. L. *Mater. Res. Bull.* **32**(2), 159–163 (1997).

30. Caldwell, M. A., Raoux, S., Wang, R. Y., Wong, H.-S. P., and Milliron, D. J. *J. Mater. Chem.* **20**(7), 1285–1291 (2010).

31. Ie, S. Y., Bea, B. T., Ahn, Y.-k., Chang, M. Y., You, D. G., Cho, M. H., Jeong, K., Oh, J.-H., Koh, G.-H., and Jeong, H. *Appl. Phys. Lett.* **90**(25), 251917 (2007).

32. Wagner, T., Orava, J., Prikryl, J., Kohoutek, T., Bartos, M., and Frumar, M. *Thin Solid Films* **517**(16), 4694–4697 (2009).

33. Hu, D., Zhu, J., and Lee, J. *Integr. Ferroelectr.* **84**(1), 233–238 (2006).

34. Němec, P., Moreac, A., Nazabal, V., Pavlišta, M., Prikřyl, J., and Frumar, M. *J. Appl. Phys.* **106**(10), 103509 (2009).

35. Braun, W., Shayduk, R., Flissikowski, T., Ramsteiner, M., Grahn, H. T., Riechert, H., Fons, P., and Kolobov, A. *Appl. Phys. Lett.* **94**(4), 041902 (2009).

36. Shayduk, R. and Braun, W. *J. Cryst. Growth* **311**(7), 2215–2219 (2009). The 15th International Conference on Molecular Beam Epitaxy (MBE-XV).

37. Jung, Y., Lee, S.-H., Ko, D.-K., and Agarwal, R. *J. Am. Chem. Soc.* **128**(43), 14026–14027 (2006).

38. Wagner, R. S. and Ellis, W. C. *Appl. Phys. Lett.* **4**(5), 89–90 (1964).

39. Yoon, H., Jo, W., Lee, E., Lee, J., Kim, M., Lee, K., and Khang, Y. *J. Non-Cryst. Solids* **351**(43–45), 3430–3434 (2005).

40. Park, G.-S., Kwon, J.-H., Kim, M., Yoon, H. R., Jo, W., Kim, T. K., Zuo, J.-M., and Khang, Y. *J. Appl. Phys.* **102**(1), 013524 (2007).

41. Ohring, M. *Materials Science of Thin Films: Deposition and Structure.* Academic Press, second edition, (2002).

42. Kim, R.-Y., Kim, H.-G., and Yoon, S.-G. *Integr. Ferroelectr.* **90**(1), 80–87 (2007).

43. Longo, M., Salicio, O., Wiemer, C., Fallica, R., Molle, A., Fanciulli, M., Giesen, C., Seitzinger, B., Baumann, P., Heuken, M., and Rushworth, S. *J. Cryst. Growth* **310**(23), 5053–5057 (2008). The Fourteenth International Conference on Metalorganic Vapor Phase Epitaxy.

44. Abrutis, A., Plausinaitiene, V., Skapas, M., Wiemer, C., Salicio, O., Pirovano, A., Varesi, E., Rushworth, S., Gawelda, W., and Siegel, J. *Chem. Mater.* **20**(11), 3557–3559 (2008).

45. Kim, R.-Y., Kim, H.-G., Park, K.-W., Ahn, J.-K., and Yoon, S.-G. *Chem. Vap. Deposition* **15**(10–12), 296–299 (2009).

46. Choi, B. J., Choi, S., Shin, Y. C., Hwang, C. S., Lee, J. W., Jeong, J., Kim, Y. J., Hwang, S.-Y., and Hong, S. K. *J. Electrochem. Soc.* **154**(4), H318–H324 (2007).

47. Choi, B. J., Choi, S., Eom, T., Ryu, S. W., Cho, D.-Y., Heo, J., Kim, H. J., Hwang, C. S., Kim, Y. J., and Hong, S. K. *Chem. Mater.* **21**(12), 2386–2396 (2009).

48. Cadoff, I. and Miller, E. *Thermoelectric Materials and Devices.* Reinhold Publishing Corporation, New York, (1960).

49. Rowe, D., editor. *CRC Handbook of Thermoelectrics.* CRC, Boca Raton, Florida, USA, (1995).

50. ThinkGeek. USB Thermoelectric Cooler & Warmer - `http://www.thinkgeek.com/product/96b3/`.

51. Bell, L. E. *Science* **321**(5895), 1457–1461 (2008).

52. Heremans, J. P., Dresselhaus, M. S., Bell, L. E., and Morelli, D. T. *Nat. Nanotechnol.* **8**(7), 471–473 (2013).

53. Martín-González, M., Caballero-Calero, O., and Díaz-Chao, P. *Renew. Sus. Energ. Rev.* **24**, 288–305 (2013).

54. Dresselhaus, M., Chen, G., Ren, Z., Dresselhaus, G., Henry, A., and Fleurial, J. *JOM J. Min. Met. Mat. S.* **61**(4), 86–90 (2009).

55. Dresselhaus, M., Lin, Y., Cronin, S., Black, M., Rabin, O., and Dresselhaus, G. In *Proceedings of the Nonlithographic and Lithographic Methods for Nanofabrication MRS Symposium*, (2001).

56. Bos, J.-W. G. and Downie, R. A. *J. Phys.: Condens. Matter* **26**(43), 433201 (2014).

57. Snyder, G. J. and Toberer, E. S. *Nat. Mater.* **7**(2), 105–114 (2008).

58. Slack, G. In *CRC Handbook of Thermoelectrics,* Rowe, D., editor, 407–440. CRC (1995).

59. Kanatzidis, M. G. *Chem. Mater.* **22**(3), 648–659 (2010).

60. Hicks, L. D. and Dresselhaus, M. S. *Phys. Rev. B* **47**(19), 12727–12731 (1993).

61. Hicks, L. D. and Dresselhaus, M. S. *Phys. Rev. B* **47**(24), 16631–16634 (1993).

62. Zhao, L.-D., Dravid, V. P., and Kanatzidis, M. G. *Energy Environ. Sci.* **7**(1), 251–268 (2014).

63. Godart, C., Gonçalves, A., Lopes, E., and Villeroy, B. In *Mater. Res. Soc. Symp. Proc.*, volume 1166-N08-01, 183–193, (2009).

64. Gonçalves, A. P. and Godart, C. *Eur. Phys. J. B* **87**(2), 42 (2014).

65. Goldsmid, H. J. *Materials* **7**(4), 2577 (2014).

66. LaLonde, A. D., Pei, Y., Wang, H., and Snyder, G. J. *Mater. Today* **14**(11), 526–532 (2011).

67. Alam, H. and Ramakrishna, S. *Nano Energy* **2**(2), 190–212 (2013).

68. Vining, C. In *CRC Handbook of Thermoelectrics,* Rowe, D., editor, 329–338. CRC (1995).

69. Uher, C. In *Proc. 22nd Int. Conf. Thermoelect.*, 42–47, (2003).

70. Müchler, L., Casper, F., Yan, B., Chadov, S., and Felser, C. *Phys. Status Solidi RRL* **7**(1–2), 91–100 (2013).

71. He, J., Liu, Y., and Funahashi, R. *J. Mater. Res.* **26**(15), 1762–1772 (2011).

72. Chen, Y., Zhao, Y., and Liang, Z. *Energy Environ. Sci.* **8**(2), 401–422 (2015).

73. Gaultois, M. W., Sparks, T. D., Borg, C. K., Seshadri, R., Bonificio, W. D., and Clarke, D. R. *Chem. Mater.* **25**(15), 2911–2920 (2013).

74. Fano, V. In *CRC Handbook of Thermoelectrics,* Rowe, D., editor, 257–266. CRC (1995).

75. Zhang, H., Liu, C.-X., Qi, X.-L., Dai, X., Fang, Z., and Zhang, S.-C. *Nat. Phys.* **5**(6), 438–442 (2009).

76. Hsieh, D., Xia, Y., Qian, D., Wray, L., Dil, J. H., Meier, F., Osterwalder, J., Patthey, L., Checkelsky, J. G., Ong, N. P., Fedorov, A. V., Lin, H., Bansil, A., Grauer, D., Hor, Y. S., Cava, R. J., and Hasan, M. Z. *Nature* **460**(7259), 1101–1105 (2009).

77. Hor, Y. S., Richardella, A., Roushan, P., Xia, Y., Checkelsky, J. G., Yazdani, A., Hasan, M. Z., Ong, N. P., and Cava, R. J. *Phys. Rev. B* **79**(19), 195208 (2009).

78. Hsieh, D., Xia, Y., Qian, D., Wray, L., Meier, F., Dil, J. H., Osterwalder, J., Patthey, L., Fedorov, A. V., Lin, H., Bansil, A., Grauer, D., Hor, Y. S., Cava, R. J., and Hasan, M. Z. *Phys. Rev. Lett.* **103**(14), 146401 (2009).

79. Hasan, M. Z. and Kane, C. L. *Rev. Mod. Phys.* **82**(4), 3045–3067 (2010).

80. Moore, J. E. *Nature* **464**(7286), 194–198 (2010).

81. Qi, X.-L. and Zhang, S.-C. *Rev. Mod. Phys.* **83**(4), 1057–1110 (2011).

82. Chen, Y. L., Analytis, J. G., Chu, J.-H., Liu, Z. K., Mo, S.-K., Qi, X. L., Zhang, H. J., Lu, D. H., Dai, X., Fang, Z., Zhang, S. C., Fisher, I. R., Hussain, Z., and Shen, Z.-X. *Science* **325**(5937), 178–181 (2009).

83. Moore, J. *Nat. Phys.* **5**(6), 378–380 (2009).

84. Welker, H. *Z. Naturforsch. A* **7**, 744–749 (1952).

85. Welker, H. *Z. Naturforsch. A* **8**, 248–251 (1953).

86. Haynes, W. M., editor. *CRC Handbook of Chemistry and Physics*. CRC Press/Taylor and Francis, Boca Raton, Florida, USA, 95th edition, (2014).

87. Kasap, S. and Capper, P., editors. *Springer Handbook of Electronic and Photonic Materials*. Springer, New York, (2006).

88. Pankove, J. I. and Berkeyheiser, J. E. *Proc. IRE* **50**(9), 1976–1977 (1962).

89. Black, J., Lockwood, H., and Mayburg, S. *J. Appl. Phys.* **34**(1), 178–180 (1963).

90. Schubert, E. F. *Light-emitting Diodes*. Cambridge University Press, (2003).

91. Nathan, M. I., Dumke, W. P., Burns, G., Dill, F. H., and Lasher, G. *Appl. Phys. Lett.* **1**(3), 62–64 (1962).

92. Hall, R. N., Fenner, G. E., Kingsley, J. D., Soltys, T. J., and Carlson, R. O. *Phys. Rev. Lett.* **9**(9), 366–368 (1962).

93. Quist, T. M., Rediker, R. H., Keyes, R. J., Krag, W. E., Lax, B., McWhorter, A. L., and Zeigler, H. J. *Appl. Phys. Lett.* **1**(4), 91–92 (1962).

94. Green, M. A., Emery, K., Hishikawa, Y., and Warta, W. *Prog. Photovolt.: Res. Appl.* **17**(5), 320–326 (2009).

95. Mimura, T. *IEEE Trans. Microwave Theory Tech.* **50**(3), 780–782 (2002).

96. Ridley, B. K. and Watkins, T. B. *Proc. Phys. Soc.* **78**(2), 293 (1961).

97. Hilsum, C. *Proc. IRE* **50**(2), 185–189 (1962).

98. Gunn, J. *Solid State Commun.* **1**(4), 88–91 (1963).

99. Oliver, J., Fairman, R., Chen, R., and Yu, P. *Electron. Lett.* **17**(22), 839–841 (1981).

100. Holmes, D. E., Chen, R. T., Elliott, K. R., and Kirkpatrick, C. G. *Appl. Phys. Lett.* **40**(1), 46–48 (1982).

101. Hoshikawa, K., Nakanishi, H., Kohda, H., and Sasaura, M. *J. Cryst. Growth* **94**(3), 643–650 (1989).

102. Chen, T., Huang, T., Chen, L., and Guo, Y. *J. Cryst. Growth* **106**(23), 367–376 (1990).

103. Bourret, E. and Merk, E. *J. Cryst. Growth* **110**(3), 395–404 (1991).

104. Moss, S. and Ledwith, A., editors. *The Chemistry of the Semiconductor Industry.* Blackie & Son Ltd., Glasgow, (1987).

105. Campomanes, R. R., da Silva, J. H. D., Vilcarromero, J., and Cardoso, L. P. *J. Non-Cryst. Solids* **299-302**(Part 2), 788–792 (2002).

106. Künzel, H. *Physica B + C* **129**(1-3), 66–80 (1985).

107. Panish, M. B. and Temkin, H. *Annu. Rev. Mater. Sci.* **19**(1), 209–229 (1989).

108. Stringfellow, G. B. *Organometallic vapor phase epitaxy - theory and practice.* Academic Press, San Diego, (1999).

109. Goodman, C. H. L. and Pessa, M. V. *J. Appl. Phys.* **60**(3), R65–R82 (1986).

110. Usui, A. and Watanabe, H. *Annu. Rev. Mater. Sci.* **21**(1), 185–219 (1991).

111. Ozeki, M. *Mater. Sci. Rep.* **8**(3), 97–146 (1992).

112. Suntola, T. and Antson, J. (1977). US Patent 4,058,430.

113. Ahonen, M., Pessa, M., and Suntola, T. *Thin Solid Films* **65**, 301–307 (1980).

114. Knez, M., Nielsch, K., and Niinistö, L. *Adv. Mater.* **19**(21), 3425–3438 (2007).

115. Leskelä, M., Niinistö, J., and Ritala, M. In *Comprehensive Materials Processing,* Hashmi, S., Batalha, G. F., Tyne, C. J. V., and Yilbas, B., editors, 101–123. Elsevier, Oxford (2014).

116. Miikkulainen, V., Leskelä, M., Ritala, M., and Puurunen, R. L. *J. Appl. Phys.* **113**(2), 021301 (2013).

117. Ritala, M. and Leskelä, M. In *Deposition and Processing of Thin Films,* Nalwa, H., editor, volume 1 of *Handbook of Thin Film Materials*, chapter 2, 103–159. Academic Press (2003).

118. Leskelä, M. and Ritala, M. *Angew. Chem. Int. Ed.* **42**(45), 5548–5554 (2003).

119. Knoops, H. C. M., Langereis, E., van de Sanden, M. C. M., and Kessels, W. M. M. *J. Electrochem. Soc.* **157**(12), G241–G249 (2010).

120. Henke, T., Knaut, M., Hossbach, C., Geidel, M., Rebohle, L., Albert, M., Skorupa, W., and Bartha, J. W. *ECS J. Solid State Sci. Technol.* **4**(7), P277–P287 (2015).

121. George, S. M. *Chem. Rev.* **110**(1), 111–131 (2010).

122. Hatanpää, T., Ritala, M., and Leskelä, M. *Coord. Chem. Rev.* **257**(23–24), 3297–3322 (2013).

123. Leskelä, M., Niinistö, L., Niemelä, P., Nykänen, E., Soininen, P., Tiitta, M., and Vähäkangas, J. *Vacuum* **41**(4-6), 1457–1459 (1990).

124. Asikainen, T., Ritala, M., and Leskelä, M. *Appl. Surf. Sci.* **82/83**, 122–125 (1994).

125. Pore, V., Ritala, M., and Leskelä, M. *Chem. Vap. Deposition* **13**(4), 163–168 (2007).

126. Szczerbakow, A., Godlewski, M., Dynowska, E., Ivanov, V. Y., Świątek, K., Goldys, E. M., and Phillips, M. R. *Acta Phys. Pol. A* **97**(3), 579–582 (1998).

127. Tammenmaa, M., Antson, H., Asplund, M., Hiltunen, L., Leskelä, M., Niinistö, L., and Ristolainen, E. *J. Cryst. Growth* **84**, 151–154 (1987).

128. Johansson, J., Kostamo, J., Karppinen, M., and Niinistö, L. *J. Mater. Chem.* **12**, 1022–1026 (2002).

129. Suntola, T., Antson, J., Pakkala, A., and Lindfors, S. In *SID International Symposium in San Diego, California, 29 April-1 May 1980, Digest of Technical Papers*, 108–109 (SID, Los Angeles, California, 1980).

130. Tadokoro, T., Ohta, S., Ishiguro, T., Ichinose, Y., Kobayashi, S., and Yamamoto, N. *J. Cryst. Growth* **130**, 29–36 (1993).

131. Ezhovskii, Y. K. and Klyuikov, A. I. *Zr. Prikl. Khim.* **73**, 881–884 (2000). [Russ. J. Appl. Chem. **73**, 933 (2000)].

132. Yao, T. and Takeda, T. *Appl. Phys. Lett.* **48**(2), 160–162 (1986).

133. Guziewicz, E., Godlewski, M., Kopalko, K., Łusakowska, E., Dynowska, E., Guziewicz, M., Godlewski, M. M., and Phillips, M. *Thin Solid Films* **446**, 172–177 (2004).

134. Feng, Y. Z. and Guo, S. P. *J. Mater. Sci. Lett.* **15**, 1824–1827 (1996).

135. Hartmann, J. M., Cibert, J., Kany, F., Mariette, H., Charleux, M., Alleysson, P., Langer, R., and Feuillet, G. *J. Appl. Phys.* **80**, 6257–6265 (1996).

136. Hartmann, J. M., Charleux, M., Mariette, H., and Rouvière, J. L. *Appl. Surf. Sci.* **112**, 142–147 (1997).

137. Herman, M. A., Jylhä, O., and Pessa, M. *J. Cryst. Growth* **66**, 480–483 (1984).

138. Faschinger, W., Hauzenberger, F., Juza, P., Pesek, A., and Sitter, H. *J. Electron. Mater.* **22**, 497–500 (1993).

139. Hartmann, J. M., Feuillet, G., Charleux, M., and Mariette, H. *J. Appl. Phys.* **79**, 3035–3041 (1996).

140. Hsu, C.-T. *Jpn. J. Appl. Phys., Part 1* **35**, 4476–4479 (1996).

141. Yokoyama, M., Chen, N. T., and Ueng, H. Y. *J. Cryst. Growth* **212**, 97–102 (2000).

142. Rees, W. S., Green, D. M., Anderson, T. J., Bretschneider, E., Pathangey, B., Park, C., and Kim, J. *J. Electron. Mater.* **21**, 361–366 (1992).

143. Koukitu, A., Saegusa, A., Kitho, M., Ikeda, H., and Seki, H. *Jpn. J. Appl. Phys., Part 2* **31**, L2165–L2168 (1992).

144. Bisengaliev, R. A., Novikov, B. V., Aleskovskii, V. B., Drozd, V. E., Ageev, D. A., Gubaidullin, V. I., and Savchenko, A. P. *Fiz. Tverd. Tela* **40**, 820–821 (1998). [Phys. Solid State **40**, 754 (1998)].

145. Bhat, I., Ehsani, H., Wang, W. S., Ghandhi, S. K., and Karam, N. H. *J. Vac. Sci. Technol. B* **10**, 1376–1379 (1992).

146. Karam, N. H., Wolfson, R. G., Bhat, I. B., Ehsani, H., and Gandhi, S. K. *Thin Solid Films* **225**, 261–264 (1993).

147. Wang, W.-S., Ehsani, H., and Bhat, I. *J. Electron. Mater.* **22**, 873–878 (1993).

148. Emerson, R. M., Hoyt, J. L., and Gibbons, J. F. *Appl. Phys. Lett.* **65**, 1103–1105 (1994).

149. Dakshinamurthy, S. and Bhat, I. *J. Electron. Mater.* **27**(6), 521–526 (1998).

150. Wang, W.-S., Ehsani, H. E., and Bhat, I. B. *J. Cryst. Growth* **124**, 670–675 (1992).

151. Hiltunen, L., Leskelä, M., Mäkelä, M., Niinistö, L., Nykänen, E., and Soininen, P. *Thin Solid Films* **166**, 149–154 (1988).

152. Kim, H. *J. Vac. Sci. Technol. B* **21**, 2231–2261 (2003).

153. Usui, A., Sunakawa, H., Stützler, F. J., and Ishida, K. *Appl. Phys. Lett.* **56**(3), 289–291 (1990).

154. McDermott, B. T., Reid, K. G., El-Masry, N. A., Bedair, S. M., Duncan, W. M., Yin, X., and Pollak, F. H. *Appl. Phys. Lett.* **56**, 1172–1174 (1990).

155. Hirose, S., Yamaura, M., and Munekata, H. *Appl. Surf. Sci.* **150**, 89–94 (1999).

156. Ishii, M., Iwai, S., Kawata, H., Ueki, T., and Aoyagi, Y. *J. Cryst. Growth* **180**, 15–21 (1997).

157. Thompson, P. E., Davis, J. L., Waterman, J., Wagner, R. J., Gammon, D., Gaskill, D. K., and Stahlbush, R. *J. Appl. Phys.* **69**, 7166–7172 (1991).

158. Koukitu, A., Nakai, H., Saegusa, A., Suzuki, T., Nomura, O., and Seki, H. *Jpn. J. Appl. Phys.* **27**(5A), L744 (1988).

159. Ahopelto, J., Kattelus, H. P., Saarilahti, J., and Suni, I. *J. Cryst. Growth* **99**, 550–555 (1990).

160. Bedair, S. M., Tischler, M. A., Katsuyama, T., and El-Masry, N. A. *Appl. Phys. Lett.* **47**(1), 51–53 (1985).

161. Dapkus, P. D., DenBaars, S. P., Chen, Q., Jeong, W. G., and Maa, B. Y. *Prog. Cryst. Growth. Charact. Mater.* **19**, 137–147 (1989).

162. Ishizaki, M., Kano, N., Yoshino, J., and Kukimoto, H. *Jpn. J. Appl. Phys., Part 2* **30**, L435–L436 (1991).

163. Kitahara, K., Ohtsuka, N., Ashino, T., Ozeki, M., and Nakajima, K. *Jpn. J. Appl. Phys., Part 2* **32**, L236–L238 (1993).

164. Ozeki, M., Haraguchi, T., and Fujita, A. *J. Cryst. Growth* **298**, 90–93 (2007).

165. Fujii, K., Suemune, I., Koui, T., and Yamanishi, M. *Appl. Phys. Lett.* **60**, 1498–1500 (1992).

166. Tran, C. A., Masut, R. A., Brebner, J. L., and Leonelli, R. *Appl. Phys. Lett.* **62**, 2375–2377 (1993).

167. Arès, R., Hu, J., Yeo, P., and Watkins, S. P. *J. Cryst. Growth* **195**, 234–241 (1998).

168. Nishizawa, J., Abe, H., and Kurabayashi, T. *J. Electrochem. Soc.* **132**(5), 1197–1200 (1985).

169. Usui, A. *Proc. IEEE* **80**(10), 1641–1653 (1992).

170. Sakuma, Y., Ozeki, M., Ohtsuka, N., and Kodama, K. *J. Appl. Phys.* **68**(11), 5660–5664 (1990).

171. Arès, R., Watkins, S. P., Yeo, P., Horley, G. A., O'Brien, P., and Jones, A. C. *J. Appl. Phys.* **83**(6), 3390–3397 (1998).

172. Mori, K., Yoshida, M., Usui, A., and Terao, H. *Appl. Phys. Lett.* **52**(1), 27–29 (1988).

173. Kobayashi, R., Jin, Y., and Hasegawa, F. *J. Cryst. Growth* **113**, 491–498 (1991).

174. Maa, B. Y. and Dapkus, P. D. *Appl. Phys. Lett.* **58**(20), 2261–2263 (1991).

175. Chen, Q., Beyler, C. A., Dapkus, P. D., Alwan, J. J., and Coleman, J. J. *Appl. Phys. Lett.* **60**(19), 2418–2420 (1992).

176. de Keijser, M. and van Opdorp, C. *Appl. Phys. Lett.* **58**(11), 1187–1189 (1991).

177. Kobayashi, R., Ishikawa, K., Narahara, S., and Hasegawa, F. *Jpn. J. Appl. Phys., Part 2* **31**, L1730–L1732 (1992).

178. Doi, A., Aoyagi, Y., and Namba, S. *Appl. Phys. Lett.* **49**(13), 785–787 (1986).

179. Wells, R. L., Pitt, C. G., McPhail, A. T., Purdy, A. P., Shafieezad, S., and Hallock, R. B. *Chem. Mater.* **1**(1), 4–6 (1989).

180. Wells, R. L. and Gladfelter, W. L. *Journal of Cluster Science* **8**(2), 217–238 (1997).

181. Schulz, S., Martinez, L., and Ross, J. L. *Adv. Mater. Opt. Electron.* **6**(4), 185–189 (1996).

182. Janik, J. F., Wells, R. L., Jr., V. G. Y., Rheingold, A. L., and Guzei, I. A. *J. Am. Chem. Soc.* **120**(3), 532–537 (1998).

183. Foos, E. E., Jouet, R. J., Wells, R. L., Rheingold, A. L., and Liable-Sands, L. M. *Journal of Organometallic Chemistry* **582**(1), 45 – 52 (1999).

184. Hatanpää, T., Pore, V., Sarnet, T., Ritala, M., and Leskelä, M. In *ALD2010. Proceedings of the 10th International Conference on Atomic Layer Deposition*, M8, (2010).

185. Huheey, J. E., Keiter, E. A., and Keiter, R. L. *Inorganic Chemistry: Principles of Structure and Reactivity*. Harper Collins College Publishers, New York, 4th edition, (1993).

186. Eom, T., Gwon, T., Yoo, S., Choi, B. J., Kim, M.-S., Buchanan, I., Xiao, M., and Hwang, C. S. *Chem. Mater.* **26**(4), 1583–1591 (2014).

187. Eom, T., Gwon, T., Yoo, S., Choi, B. J., Kim, M.-S., Buchanan, I., Ivanov, S., Xiao, M., and Hwang, C. S. *Chem. Mater.* **27**(10), 3707–3713 (2015).

188. Knapas, K., Hatanpää, T., Ritala, M., and Leskelä, M. *Chem. Mater* **22**(4), 1386–1391 (2010).

189. Waldo, R. In *Microbeam Analysis. Proceedings of the 23rd Annual Conference of the Microbeam Analysis Society,* Newbury, D., editor, 310. San Francisco Press, (1988).

190. Mäntymäki, M., Heikkilä, M. J., Puukilainen, E., Mizohata, K., Marchand, B., Räisänen, J., Ritala, M., and Leskelä, M. *Chem. Mater.* **27**(2), 604–611 (2015).

191. Raoux, S., (2012). personal communication.

192. Raoux, S., Muñoz, B., Cheng, H.-Y., and Jordan-Sweet, J. L. *Appl. Phys. Lett.* **95**(14), 143118 (2009).

193. Nilsen, O., Karlsen, O. B., Kjekshus, A., and Fjellvåg, H. *Thin Solid Films* **515**(11), 4527–4537 (2007).

194. Nilsen, O., Karlsen, O. B., Kjekshus, A., and Fjellvåg, H. *Thin Solid Films* **515**(11), 4538–4549 (2007).

195. Nilsen, O., Karlsen, O. B., Kjekshus, A., and Fjellvåg, H. *Thin Solid Films* **515**(11), 4550–4558 (2007).

196. Ritala, M., Pore, V., Hatanpää, T., Heikkilä, M., Leskelä, M., Mizohata, K., Schrott, A., Raoux, S., and Rossnagel, S. M. *Microelectron. Eng.* **86**(7–9), 1946–1949 (2009).

197. Kadel, K., Kumari, L., Li, W., Huang, J. Y., and Provencio, P. P. *Nanoscale Res. Lett.* **6**, 57 (2011).

198. Qiu, X., Austin, L. N., Muscarella, P. A., Dyck, J. S., and Burda, C. *Angew. Chem. Int. Ed.* **45**(34), 5656–5659 (2006).

199. Giani, A., Bayaz, A. A., Foucaran, A., Pascal-Delannoy, F., and Boyer, A. *J. Cryst. Growth* **236**(1-3), 217–220 (2002).